

Article

A Lightweight CNN and Class Weight Balancing on Chest X-ray Images for COVID-19 Detection

Noha Alduaiji ¹, Abeer Algarni ², Saadia Abdalaha Hamza ³, Gamil Abdel Azim ^{4,5,6,*}
and Habib Hamam ^{6,7,8,9}

- ¹ Department of Computer Science, College of Computer and Information Sciences, Majmaah University, Al-Majmaah 11952, Saudi Arabia
 - ² Department of Information Technology, College of Computer and Information Sciences, Princess Nourah bint Abdulrahman University, P.O. Box 84428, Riyadh 11671, Saudi Arabia
 - ³ Department of Computer Science, College of Science and Humanities—Slayel, Prince Sattam Bin AbdulAziz University, Al-Kharj 16278, Saudi Arabia
 - ⁴ Department of Computer Science, Faculty of Computers and Information, Canal Suez University, Ismailia 8366004, Egypt
 - ⁵ AI Department, Ascent College, Montreal, QC H2P2X2, Canada
 - ⁶ Faculty of Engineering, Université de Moncton, Moncton, NB E1A3E9, Canada
 - ⁷ International Institute of Technology and Management, Commune d’Akanda, Libreville P.O. Box 1989, Gabon
 - ⁸ School of Electrical Engineering, Department of Electrical and Electronic Engineering Science, University of Johannesburg, Johannesburg 2006, South Africa
 - ⁹ Spectrum of Knowledge Production and Skills Development, Sfax 3027, Tunisia
- * Correspondence: Gazim3@gmail.com

Abstract: In many locations, reverse transcription polymerase chain reaction (RT-PCR) tests are used to identify COVID-19. It could take more than 48 h. It is a key factor in its seriousness and quick spread. Images from chest X-rays are utilized to diagnose COVID-19. Which generally deals with the issue of imbalanced classification. The purpose of this paper is to improve CNN’s capacity to display Chest X-ray pictures when there is a class imbalance. CNN Training has come to an end while chastening the classes for using more examples. Additionally, the training data set uses data augmentation. The achievement of the suggested method is assessed on an image’s two data sets of chest X-rays. The suggested model’s efficiency was analyzed using criteria like accuracy, specificity, sensitivity, and F1 score. The suggested method attained an accuracy of 94% worst, 97% average, and 100% best cases, respectively, and an F1-score of 96% worst, 98% average and 100% best cases, respectively.

Keywords: machine learning; transfer learning; class weight balancing; convolution neural networks; COVID-19



check for updates

Citation: Alduaiji, N.; Algarni, A.; Abdalaha Hamza, S.; Abdel Azim, G.; Hamam, H. A Lightweight CNN and Class Weight Balancing on Chest X-ray Images for COVID-19 Detection. *Electronics* **2022**, *11*, 4008. <https://doi.org/10.3390/electronics11234008>

Academic Editor: Panagiota Spyridonos

Received: 30 October 2022
Accepted: 29 November 2022
Published: 2 December 2022

Publisher’s Note: MDPI stays neutral with regard to jurisdictional claims in published maps and institutional affiliations.



Copyright: © 2022 by the authors. Licensee MDPI, Basel, Switzerland. This article is an open access article distributed under the terms and conditions of the Creative Commons Attribution (CC BY) license (<https://creativecommons.org/licenses/by/4.0/>).

1. Introduction

The COVID-19 pandemic is deadly and extremely severe. It is one of the main problems of the twenty-first century. In March 2020, the World Health Organization (WHO) declared COVID-19 to be a pandemic [1]. It exhibits signs and symptoms like those of pneumonia [2]; however, it is more fatal. To reduce the transmission of COVID-19 infection [3,4], suitable safety measures are needed.

The most widely used molecular type test for COVID-19 detection in people is the Reverse Transcription Polymerase Chain Reaction (RT-PCR). It is the gold standard for diagnosing Coronavirus [5]. Within three weeks of the onset of symptoms, an RT-PCR test has a 90% accuracy in identifying COVID-19 circumstances favorably [6]. The RT-PCR test does, however, have many drawbacks. It is not very widely available, and obtaining the test results takes longer than 48 h.

Although RT-PCR [7] is the first and most efficient approach for detecting COVID-19, this procedure is rather time-consuming. It might take hours or even days and require

special packages that are only sometimes available in far-flung parts of a country because of geological, social, and economic factors. The rapid antigen test, on the other hand, examines a nasal swab for the presence of infection-related antigens, but has a higher probability of errors. The serological test looks for antibodies the body's immune system has developed to fight the illness from the person's blood. However, it examines just one IgM and one IgG antibody during or after recovery, making it inefficient for extremely early viral identification.

Vaccinations have either Food and Drug Administration (FDA) or European Medicines Agency (EMA) authorization [8]. CT scans and chest X-rays are two typical chest radiography procedures. Both have pros and cons, but a chest X-ray costs less than a CT scan because it uses less expensive equipment. When molecular tests, such as RT-PCR, are not accessible or time is restricted, COVID-19 can be identified rapidly and correctly by analyzing individual chest radiographs [9].

Many doctors and radiologists agree that chest X-rays can find COVID-19, which has the same 90% accuracy as the RT-PCR test. CT scans and chest X-rays have distinct positive and negative attributes. A CT scan requires more expensive equipment than a chest X-ray. In addition, the disinfection time for a CT scan is around 15 min, which is significantly longer than a chest X-ray because a portable version exposes the patient to fewer germs. Additionally, the person obtains more ionizing radiation from a CT scan than from a chest X-ray. Chest X-rays comprise the bulk of routine radiology examinations. Hundreds of millions of these photos are taken annually in hospitals and clinics worldwide to help doctors figure out what is wrong with people. CT and X-ray scans use parts of the electromagnetic spectrum that cannot be seen to find problems very early on. This has a lot of medical value. Chest X-rays are better than CT scans because they are more common in hospitals and expose patients to less ionizing radiation. CT and X-ray scans, which have a high scientific value, use unseen forms of the electromagnetic spectrum to detect abnormalities for early detection [9].

In this research, we discovered that chest X-ray examinations are inexpensive, and the results are straightforward. Chest X-ray tests are administered easily. It offers portable variants with a decreased danger of radiation exposure. It makes X-ray scans easier to use than CT scans. CT scans, on the other hand, expose people to a lot of radiation, cost a lot, require clinical expertise, and cannot be moved.

Machine learning (ML) applications in healthcare are prevalent [10,11]. To find out if a person has a COVID-19 infection, RTPCR testing [7], X-ray imaging [12–15], computed tomography (CT) scanning [2], rapid antigen detection [16], and serological testing [17] are all used.

Since beating the world champion at Go [18], the completion of a fill-in-the-blank text [19], and robotic hand control to solve the Rubik's cube [20], deep learning has gained popularity.

Due to the present COVID-19 epidemic, several efforts are being made to identify and combat it. Recent advancements in computer vision have paved the way for applying deep learning and convolutional neural networks to medical image diagnosis, such as retinopathy identification [21–25] and tumor discovery [26–28]. Numerous research studies have been published in this field to combat COVID-19.

The use of deep learning in the battle against COVID-19 seems promising [29,30]. Still, it is important to be aware of the problems with deep learning, such as how hard it is to understand, how generalization metrics work, how learning from limited, labeled data sets affects data privacy, and so on [31].

In the Section 2, we talk about a few recent studies that used chest X-rays and CT scans to look for COVID-19. This work improved the CNN lightweight and class balance for COVID-19 identification from chest X-rays.

We tried out different data sets with different requirements (see Section 4.1, and the learning technique did the parametric workout for efficient parameter selection and change. The results demonstrate that the proposed model is more accurate than existing

cutting-edge approaches. In the end, the tuning and training produce an excellent design configuration that reveals the fundamental behavior of the architecture's characteristics.

Deep learning technologies are a good way to build automated systems to help radiologists understand chest X-ray images. Chest X-rays are an important and easy-to-obtain way to diagnose many diseases affecting the thorax [32,33].

The following are the essential contributions to this work:

- Proposed a unique lightweight CNN model and the balance of the class for COVID-19 identification from chest X-ray pictures.
- The proposed model was looked at using a medium-sized data set of chest pictures and augmentation data.
- Used class weight balancing to solve a problem involving imbalanced classes.
- A CNN lightweight that has been fine-tuned and is the class average for chest X-ray pictures.
- Evaluating data sets experimentally using different specifications (results section), where the learning process changed the exercises for choosing and adjusting parameters efficiently.
- The outcomes validate the suggested model, which is more precise than existing state-of-the-art methods. In the end, tweaking and training lead to a design configuration that looks good and explains how the parameters that went into making it work.

This work contains five sections. In Section 2, the related work is discussed. Section 3 goes into detail about the proposed model and the data set that was used to test it. Section 4 compares the results of the recommended model to those of recent research. The study is concluded in Section 5, which covers future research.

2. Related Work

This section presents the commonly related techniques to detect the COVID-19 virus.

There are numerous proposed techniques to detect the COVID-19 virus. For example, in [34], Apostolopoulos and Mpesiena employed transfer learning with a data set of healthy, pneumonia, and COVID-19 X-ray pictures to create their model. In [35], Ozturk et al. create a deep network employing the DarkNet model. The model includes 17 convolution layers and employs the Leaky ReLU activation function; they obtain an accuracy of 98.08% for binary classes and 87.02% for multi-class cases. In [36], Waheed et al. developed a model called CovidGAN (Auxiliary Generative Adversarial Network for Classifier) to develop synthetic X-ray images and enhance the COVID-19 classification accuracy. In [37], Sathy et al. designed an exclusive feature for a support vector machine-based method. They examined SVM with different CNN models for COVID-19 identification. In [13], Hemdan et al. developed the COVIDX-Net, which includes seven different structure models of deep convolution neural networks (VGG19 and Google MobileNet V2). They employed 150 images of chest X-rays, including 25 positive COVID-19 samples. In [38], Qaid et al. employ deep models and transfer learning to develop general, robust models for COVID-19 identification. In [39], Abdulkareem and Mpesiena developed a model to identify COVID-19 based on machine learning and IoT in smart hospitals. Khorami et al., in [40], developed a method to derive the characteristics of X-ray images based on a gray-level co-occurrence matrix and Discrete Wavelet Transform (DWT), then classified the images using an improved CNN model by the Red Fox Optimization algorithm. In [41], Fareed et al. employed deep CNN models such as ResNet50, MobileNet, InceptionV3 and X-ray images. In [42], Abbas et al. studied a deep CNN called DeTraC (Decompose, Transfer, then Compose) to classify pictures from COVID-19 chest X-rays with an accuracy of 93.1%.

Recently, Rehman et al. [43] released a study titled "COVID-19 Detection Enabled by Machine Learning and Deep Learning Techniques." In [43], the authors focus on completing two tasks; the first is an analysis of recently published ML/DL techniques related to the detection of coronaviruses, and the second is a consideration of upcoming research challenges; additionally, they determine the significance of available data sets from

the literature used for the prediction of COVID-19, analyzing the ML and DL techniques used to detect COVID-19, and identifying the directions of future research. The authors of [43] offer various learning types employed in deep learning systems to combat COVID-19. The authors of [43] present a variety of algorithm-classifiers and their accuracy performance on various data sets. We recommend that readers investigate.

A survey on deep learning solutions for COVID-19 was published by Shorten et al. [31]. It focuses on progressing technological solutions, emphasizing deep learning. Their studies propose and discuss some elements, such as the capability of solving, the current state of this technology, and the COVID-19 formulation as the application of deep learning for fighting COVID-19 in many ways. We suggest to the readers explore [31]. Zhou et al. [32] proposed an intra- and inter-contrastive attention model and a chest radiology knowledge graph to enhance the efficiency of thoracic disease diagnosis. Zhou et al. [33] proposed a many-to-one distribution learning and a K-nearest neighbor smoothing method to enhance the efficiency of thoracic disease diagnosis, where COVID-19 disease is among the thoracic diseases. The work of Zhou et al. is useful to apply for the COVID-19 disease diagnosis, which is our attention in our future works. Additionally, the investigation of the suggested model is a lightweight CNN and class weight balancing on images of Chest X-ray for thoracic disease diagnosis. (L-CNN-CWB-CX).

A systematic evaluation of the literature and future directions for analyzing and diagnosing the COVID-19 epidemic using deep learning was published by Heidari A. et al., in [44]. Long Short-Term Memory Networks (LSTM), Self Organizing Maps (SOM), Conventional Neural Networks (CNNs), Generative Adversarial Networks (GANs), Recurrent Neural Networks (RNNs), Autoencoders, and Hybrid Class are the seven categories into which they divide the DL techniques used to combat COVID-19. The advantages and disadvantages of each class are also presented.

In [45], Park et al. create a model to combat and identify COVID-19; they combine a self-supervised learning approach with convolution attention to solve the classification problem. More than 100,000 chest X-Ray pictures with a structural similarity index (SSIM) were used in self-supervised learning utilizing a U-shaped CNN model in conjunction with a convolution block attention model (CBAM). Their approach model provides an exceptionally high precision normal, pneumonia, and COVID-19 categorization. Their suggested model has excellent classification performance, evidenced by the COVID-19 class's average AUC (area under the curve) of 0.994. In [46], Nasiri and Hasani used DenseNet169 to extract characteristics of X-ray images and employed XGBoost for classification; the accuracy is 89.70% and 98.24% in multi-class and binary classification.

Heidari et al. [47] describe a model that uses blockchain-based Convolutional Neural Networks to train a global DL model using a modest amount of data (chest CT images) from multiple sources, such as companies or areas of hospitals (CNNs). They make use of the Transfer Learning (TL) methodology. In terms of precision (2.7%), recall (3.1%), F1 (2.9%), and accuracy (2.8%), they show that their strategy performs better on average than state-of-the-art methods. To alleviate the overfitting issue, Zheng et al. suggest a two-stage training method in [48]. This method enhances the generalization capacity of deep CNN by optimizing the feature boundary and is robust to the selection of hyper-parameters.

In the following Sections 2.1–2.3, we present the commonly related works to the subjects CNN with medical image classification, Pneumonia and COVID-19 Medical diagnosis using chest X-ray images.

2.1. CNN and Medical Image Classification

CNN is among the most attractive DNNs. It has a lot of hidden layers that do sampling and convolution to reduce the quantity of data that comes in. This network is highly effective in diverse areas, especially computer vision [49]. Convolution layers constitute CNN, and the following convolution layers' data sources and outputs are attribute vectors. Every layer includes several networks that are highly complex. The depth of the resulting feature mappings is equivalent to that of the convolution task's multiple filters [50]. In [51],

the authors show how chest X-rays can be used to find and predict tuberculosis using simple CNN architectures.

2.2. Pneumonia and COVID-19

A variety of bacteria and viruses can cause pneumonia. General radiologists in the network of emergency hospitals have to look at many chest X-rays to find something unexpected. That can be time-consuming and difficult. During this pandemic, radiologists have been asking more and more about COVID-19 contamination pneumonia. That is because there are many similarities between COVID-19 contamination pneumonia and other pathogens or viruses [52].

Using computer systems, researchers tested several intelligent strategies for detecting the COVID-19 infection. Ground-glass opacity is identified using ultraviolet imaging of the lungs [53,54].

In an extension phase, individuals suffering from Dynamic Pneumonia can result in intense respiratory distress disorder, as this infection primarily assaults the individuals' respiratory system [55]. Researchers applied numerous computer vision and deep learning approaches to categorizing the patients with this transmittable disease from healthy people [51,56,57].

Researchers primarily focused on identifying the severity of the disease by analyzing chest X-ray pictures [58], chest CT scan images [59], or cough audio recognition [60].

Consequently, several deep learning models described in the literature try to determine COVID-19 cases. Although some deep learning-based CNN designs are applied to CT pictures, further research has used CNN models, such as DarkCovidNet [35] and COVIDX-Net [13], to identify and classify COVID-19 cases using chest X-ray images. Medical imaging is reliable and essential for efficiently regulating the spread of COVID-19 and treating patients to reduce mortality [14]. Ai et al. [61] discovered that upper body CT scans detect COVID-19 infections much quicker than RT-PCR tests.

Regular scanning could be helpful for keeping an eye on how well someone is getting better or how bad their illness is. Li and his colleagues [62] made a COVNet architecture based on deep learning to sort CT scan images by COVID-19, pneumonia, and other lung diseases. Li and Xia [63] utilized breast CT images of COVID-19 patients. They compared them to clients who were not infected to find out if the patterns of infection were the same and to reduce the falsely favorable pricing in their results. Wang et al. [59] used an extra-deep discovery technique for chest CT images and pathological visual exams to find COVID-19.

Chest X-ray radiography is often employed in medical techniques because of its inexpensive, reduced radiation portion, user-friendly and vast ease of access benefits as a whole or neighborhood health centers [64].

2.3. A Medical Diagnosis of COVID-19 Using Chest X-ray Images

Sethy et al. [37] came up with a way to use X-ray images and deep learning to find a COVID-19 infection with 95.38% accuracy. In the same way, Apostolopoulos and Mpe-siana [34] suggested for COVID-19 an X-ray image deep learning model that was 98% accurate. Ozturk et al. [35] implemented two deep learning-based methods for binary categories (COVID-19 and non-COVID-19) and three-way categories (COVID-19, normal, and pneumonia), reaching 98.08% and 87.02% accuracy, respectively. Oh et al. [57] used a logical approach to figure out how likely it was that X-ray COVID-19 pens would break. They cooperated on a regional patch-based technique utilizing chest morphology, mean chest, intensity, and standard deviation of chest endurance in five classes: normal lungs, tuberculosis, pneumonia, viral pneumonia, tuberculosis, and COVID-19. Their design achieved the highest classification accuracy of up to 88.9%. Azemin et al. [58] came up with a deep learning-based forecasting method that could tell the difference between COVID-19 and normal chest X-rays with an accuracy of 71.9%.

Heidari et al. [56] showed a chest X-ray to find COVID-19 and figure out how serious the health problem is. They obtained around 8474 chest X-rays and divided them into three

groups: non-pneumonia, COVID-19-contaminated pneumonia, and other community-acquired pneumonia that was not contaminated by COVID-19. Asnaoui et al. [65] looked at CT and X-ray images of the chest and used a model called inception-ResNetV2. They obtained the best category accuracy of 92.18% for COVID-19 normal and pneumonia cases.

In DenseNet 121-COVID-19, Ezzat uses the Gravitational Search Algorithm (GSA) to fight COVID-19 instances with a 98.38% percent accurate chest X-ray [66]. Kumar et al. [67] show a method to use the Gray Level Co-occurrence Matrix Feature (GLCM) and the Zernike Moment Feature (ZMF) together. They utilize a 36-feature Zernike Moment algorithm with texture contrast and variance. Their implementation's performance displays an accuracy rate of 93.4%. Shorten C et al. [31] published a deep learning application for the COVID-19 survey. They present deep learning applications to fight in different domains such as natural languages processing [68–74], Literature Mining [15,75–77], Misinformation Detection [78–82], Public Sentiment Analysis [83,84], Life sciences [85], Precision Diagnostics [86], Protein structure prediction [87,88], Drug re-purposing [89], Computer vision [69,90–93], Ambient Intelligence [90,94], Vision-based robotics [95,96], Medical Image Analysis [93,97], Epidemiology, Black-box spread forecasting [98], SIR models [99,100], and Contact Tracing [101]. In [31], the authors describe the present circumstances of deep learning limitations of COVID-19 detection. We refer readers to [31] for more information. Zhao et al. [102] propose a faster mean-shift technique for segmenting and tracking cells. In [103], VoxelEmbed is an embedding-based deep learning method that Zhao et al. created to separate and track 3D cell occurrences. The authors in [104] build and use a generative adversarial network model called “D+GAN” to translate faces from one image to another under multiple conditions.

The Mobile NetV2 model and a chest X-ray were used by Ragab M. and his associates to successfully identify COVID-19 with 95.8% accuracy [30].

Akbar et al. [105] write about the benefits of using machine learning and deep learning together to find and get rid of COVID-19. They discuss CNN's use of pre-trained, well-known, cutting-edge deep-learning models. They talk about different ways to classify CX photos and how deep-learning models can be used to pick out and improve certain features. They also show that deep learning models are accurate between 93% and 98% of the time when chest X-rays are used to find COVID-19.

3. Materials and Methods

In this section, Materials and Methods, we describe all data sets that are used in Section 3.1, Convolutional Neural Networks (CNN) in Section 3.2, the proposed CWB-CX model of CNN architecture in Section 3.2.1, and data augmentation in Section 3.3.

3.1. Data Set Description

Data set 1 consists of Chest X-rays with only 102 images of clients diseased with Coronavirus. We incorporated just 414 images from the Normal group. The data set establishes data accumulated from different two open-source databases taken from:

- GitHub database [62];
- Kaggle dataset, which includes 8851 normal and 6012 infected with pneumonia samples (<https://kaggle.com/c/rsna-pneumonia-detection-challenge> (accessed on 10 September 2022)).

The second data set includes 1583 normal, 576 COVID-19, and 4273 pneumonia pictures. We exclude pneumonia and make use of COVID-19 and normal chest images [106]. Our principal investigation focuses on COVID-19 with a medium size data set of chest images concurrently with data augmentation techniques. In Figures 1–3, we present the images distribution of each class in data set 1 and data set 2 and chest image, respectively.

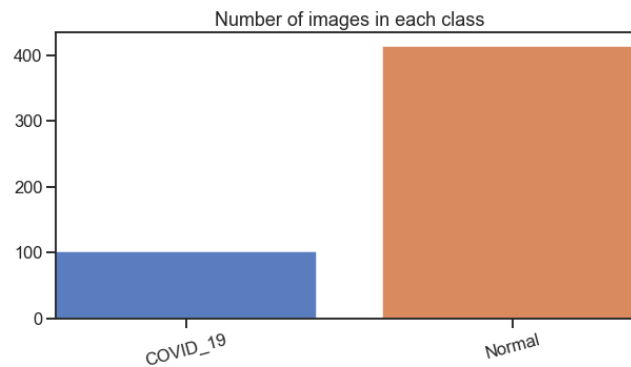


Figure 1. The proportion of each class's data in the data set 1.

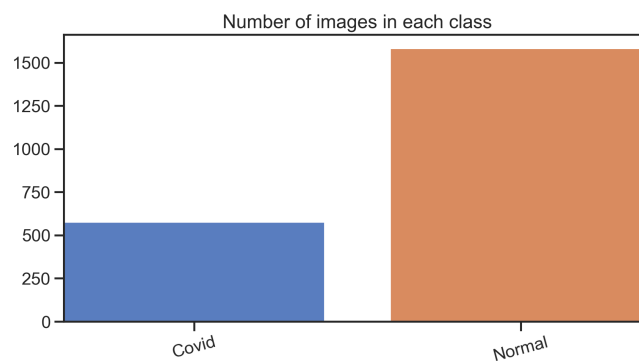


Figure 2. The proportion of each class's data in the data set 2.

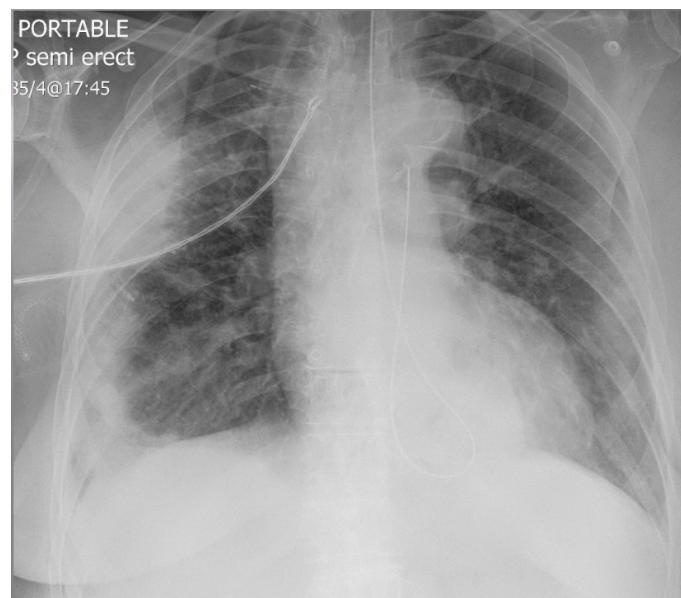


Figure 3. Example of X-ray images.

3.2. Convolution Neural Networks (CNN)

Initially, LeCunetal created CNN's approach for classifying handwritten digit image data [62]. CNN is built on layers called convolution (Conv), pooling, the rectified linear unit (ReLU) equation, fully connected (FC), batch normalization (BN), and global pooling (GP) [50]. CNN employs a mathematically unique convolution process in at least one layer. When convolution and neural networks are used together, applications for segmentation, feature extraction, noise removal, augmentation, and classification work better. CNN

is used to train the convolution filters, which are initialized randomly. CNN uses local receptive fields, weight sharing, and subsampling in its designs [51]. In clinical imaging applications, trained designs must be easy to understand so their accuracy can be checked. With deep learning techniques, classification performance is enhanced, but models are less interpretable. Compared to manually built features and simple machine learning classifiers, classification prediction is hard to understand because it depends on many parameters.

In the following Sections 3.2.1 and 3.3, we present the proposed CWB-CX model CNN architecture and data augmentation methods.

3.2.1. The Proposed CWB-CX Model CNN Architecture

A recommended CWB-CX-Model CNN design is based on the typical CNN architectures. A lightweight CNN version is suggested to categorize chest X-ray images into two classes, normal and COVID-19. For quick CNN design execution, the chest X-ray images are resized to $256 \times 256 \times 3$ dimensions. The chest X-ray image's pixels are each standardized to bring the intensities into a uniform range. The proposed CNN style consists of four convolution layers, each with 64, 64, 128 and 256 filters. The 2×2 kernel of each convolution layer contains a ReLU activation function. The attribute maps' dimensions are chosen under literary examples of improved efficiency. LeNet, AlexNet, VGG16, and InceptionV3 designs conform to current architectural ideas by enhancing function maps or filters to future layers. To evaluate chest X-ray images, lightweight or shallow CNN must be applied effectively with high classification precision.

This information is used in the proposed plan to build a lightweight CNN architecture with four layers for classifying chest X-rays. Layers of batch normalization and max-pooling are added to the convolution layers. For classification tasks, the linked layer is usually the last layer of the CNN architecture. This layer gives the expected probabilities for each class label [34]. The space layer is the most important part of making class-specific activation maps. Due to this, it enforces a solid correlation between attribute maps and classes. That reduces the chance of overfitting. So, according to Anderson [54], global average pooling (GAP) is the last layer in the proposed CNN design instead of being a connected layer. The average feature map of the last convolution layer is used to put chest X-ray pictures into groups. The last layer of the proposed system is meant to keep data from being lost. This will make sure that important details (information) are not lost during the space mission. The final layer that is recommended uses 256 filters and has a size of 28×28 . Figures 4 and 5 illustrate the suggested model's description.

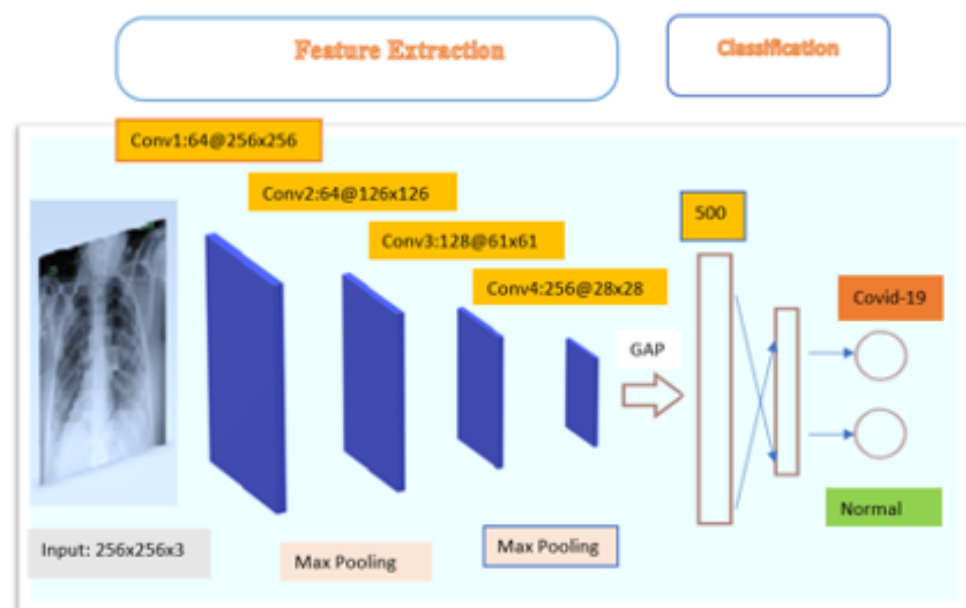


Figure 4. The proposed structure of CNN-CWB-CX.

Layer (type)	Output Shape	Param #
conv2d (Conv2D)	(None, 256, 256, 64)	832
max_pooling2d (MaxPooling2D)	(None, 128, 128, 64)	0
conv2d_1 (Conv2D)	(None, 128, 128, 64)	16448
max_pooling2d_1 (MaxPooling2D)	(None, 64, 64, 64)	0
conv2d_2 (Conv2D)	(None, 64, 64, 128)	32896
max_pooling2d_2 (MaxPooling2D)	(None, 32, 32, 128)	0
conv2d_3 (Conv2D)	(None, 32, 32, 256)	131328
max_pooling2d_3 (MaxPooling2D)	(None, 16, 16, 256)	0
flatten (Flatten)	(None, 65536)	0
dense (Dense)	(None, 500)	32768500
dense_1 (Dense)	(None, 2)	1002
=====		
Total params: 32,951,006		
Trainable params: 32,951,006		
Non-trainable params: 0		

Figure 5. Description of the proposed model.

The suggested architecture also uses CWB-CX to address the problem of class imbalance. In this strategy, classes with fewer image examples are given more weight and vice versa. The equation provided by King et al. [107,108] is used to calculate the class weights for each class.

$$W_j = \frac{N}{K * N_j} \tag{1}$$

where K is the total number of classes, W_j is the weight of class j , N is the total number of photos, and N_j is the number of images in class j . The class weights used throughout CNN Learning penalize the minority class category when it becomes the dominant class. The GAP layer’s final features employed the SoftMax activation function and were coupled to the dense layer for classification.

$$ReLU(x) = \max(0, x). \tag{2}$$

The cross-entropy loss function is commonly used in deep learning. Equations (2)–(4) [109]

$$loss(y, \hat{y}) = \frac{1}{n} \sum_{i=1}^n z_i \tag{3}$$

$$where, z_i = -(y_i \log(y_i) - (1 - y_i) \log(1 - y_i)). \tag{4}$$

W_{ij} is initialized using the Xavier uniform initializer. Utilizing the Max pooling with size = 2 and Dropout (0.3) to reduce the over-fitting, the size of the feature maps is substantially reduced by a factor of 2. With the following widely used heuristic Equation (5) [110],

we initialized the biases to be 0 and the weights W_{ij} at each layer, where $U[n, n]$ is the uniform distribution in the interval $(-n, n)$, and n is the size of the preceding layer.

Utilizing the Xavier uniform initializer, W_{ij} is initialized. When using Max pooling with size = 2, the size of the feature maps is significantly decreased by a factor of 2. The following often used a heuristic equation, where Dropout (0.3) reduces over-fitting. At each layer, we set the biases to 0 and the weights to W_{ij} , where $U[n, n]$ is the uniform distribution in the range $(-n, n)$, and n is the size of the layer before it.

$$W_{ij} \sim U\left[-\frac{1}{\sqrt{n}}, \frac{1}{\sqrt{n}}\right]. \quad (5)$$

3.3. Data Augmentation

In deep learning, Data Augmentation is a usual practice. Therefore, every deep learning framework has augmentation methods or a complete library to implement image augmentations using built-in techniques in Keras. *KerasImageDataGenerator* class offers a fast and simple way to augment images. It provides various augmentation methods like standardization, shifts, rotation, brightness change, flips, and many more. Nevertheless, the principal benefit of employing the *KerasImageDataGenerator* class is that it is developed to offer online data augmentation. It generates augmented images in the training phase of the model.

Image Augmentation with Keras ImageDataGenerator Class

The *ImageDataGenerator* class guarantees that the model receives new varieties of images on each epoch. Nevertheless, it just returns the changed images. It does not include them in the initial corpus of images. If it were the instance, then the model would certainly be seeing the initial images many times, which would over-fit the model. One more advantage is that it requires reduced memory usage. It is so because we load all the pictures without utilizing this class. Nevertheless, we are packing the images by batches on utilizing it, saving much memory. A series of methods are used, such as pixel scaling techniques. We will concentrate on five main augmentation techniques for images: photo changes using height shift and size shift range disagreements, the image flips using vertical flip and horizontal flip arguments, image rotations using the rotation range disagreement, image illumination via the illumination arguments disagreement and image zoom through the zoom range argument. A sample of data augmentation operations is shown in Figure 6.

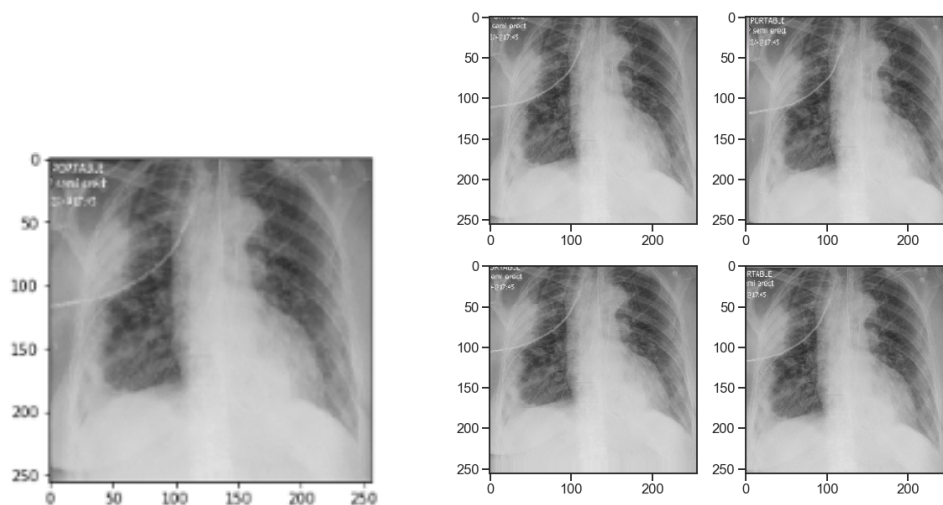


Figure 6. Data augmentation.

4. Experimental Setup and Environment

In this section, Experimental Setup and Environment, we present the results and discussion (Section 4.1), results data set 2 (Section 4.2) and complexity of the proposed model.

The model that was suggested was built using the Keras library [111] on the TensorFlow backend [112] on Windows 10, which is a working 64-bit framework. The model was executed with Python (free Python). The following is the foundation for investigation: Intel R Center i7-8250U CPU @ 1.70 GHz, 1900 MHz, 7 Cores. There were 16 GB of memory and nine consistent Pr. In the proposed architecture, the final feature vector from the GAP layer is sent to the dense layer, which has two neurons, one for each class. The following is the foundation for investigation: Intel R Center i7-8250U CPU @ 1.70 GHz, 1900 MHz, 7 Cores. There were 16 GB of memory and nine consistent Pr. In the proposed architecture, the final feature vector from the GAP layer is sent to the dense layer, which has two neurons, one for each class. The data collection was previously partitioned into training and testing sets. The training set of data sets is divided into training and validation sets (beginning at 60% and increasing by 10%), 60%, 70%, 80% and 40%, 30%, 20%, with X-ray scans of the chest in each pair, accordingly.

In Figures 1 and 2, you can see how the images in each data set are spread out. For each training session, a batch size of 32 is used to train the model. The model is trained on the categorical cross-entropy (CCE) and the binary cross-entropy (BCE) loss functions, see Equations (3) and (4). Additionally, for back-propagation, the optimizers Adam with a learning rate of 0.01 and SGD (learning rate = 0.01; momentum = 0.9) are utilized. All results are displayed in Tables 1–4. During the training phase, training and validation examples are applied with the class weights. The learning is penalized in accordance with the class-specific weights. Where the weight value of the COVID-19 class (576 samples) is 1.874, the weight value of the normal class (1583 samples) is 0.682 for the data set 2, and where the weight value of the COVID-19 class (102 samples) is 2.529, and the weight value of the normal class (4 hundred and fourteen samples) is 0.623 for the data set 1.

Table 1. Adam’s rate of learning is =0.001. The loss function is categorical cross entropy (CCE).

V.S	ACC	SENS	SEPC	PREC	RECA	F1-Score	ROC	C.M	EP
0.40	97%	1.0	1.0	100.0%	95.8%	97.872%	0.98	[8 0][1 23]	30
0.40	97%	1.0	1.0	100.0%	96.3%	98.113%	0.98	[5 0][1 26]	40
0.30	94%	1.0	1.0	100.0%	92.6%	96.15%	0.96	[5 0][2 25]	30
0.20	97%	1.0	1.0	100%	95%	97.46%	0.98	[12 0][1 19]	20

V.S: Validation split, ACC: Accuracy, SENS: Sensitivity, SEPC: specificity, PREC: Precision, RECA: Recall, Roc: ROC (area), C.M: Confusion Matrix, EP: epochs.

Table 2. SGD (rate of learning 0.001; momentum = 0.9). The loss function is cross-categorical entropy (CCE).

V.S	ACC	SENS	SEPC	PREC	RECA	F1-Score	ROC	C.M	EP
0.40	100%	1.0	1.0	100%	100%	100%	1.0	[6 0][0 26]	40
0.30	94%	0.86	0.86	96.0%	96.0%	96.0%	0.91	[6 1][1 24]	40
0.20	97%	0.90	0.90	95.8%	100.0%	97.87%	0.94	[8 1][0 23]	40

V.S: Validation split, ACC: Accuracy, SENS: Sensitivity, SEPC: specificity, PREC: Precision, RECA: Recall, Roc: ROC (area), C.M: Confusion Matrix, EP: epochs.

According to the data shown in Tables 1–4, the performance of the suggested model is satisfactory.

In the following Tables 5–7, we compare the performance of state-of-the-art approaches to that of the suggested method.

Table 3. SGD (rate of learning 0.001; momentum = 0.9). The loss function is binary cross entropy (BCE).

V.S	ACC	SENS	SEPC	PREC	RECA	F1-Score	ROC	C.M	EP
0.40	97%	1.0	1.0	100%	96.0%	97.96%	0.98	[7 0][1 24]	40
0.30	97%	1.0	1.0	100%	96.43%	98.18%	0.98	[4 0][1 27]	40
0.20	97%	1.0	1.0	100%	96.0%	97.96%	0.98	[7 0][1 24]	40
0.15	97%	1.0	1.0	100%	95.46%	97.67%	0.98	[10 0][1 21]	40

V.S: Validation split, ACC: Accuracy, SENS: Sensitivity, SEPC: specificity, PREC: Precision, RECA: Recall, Roc: ROC (area), C.M: Confusion Matrix, EP: epochs.

Table 4. Adam's rate of learning is = 0.001. The loss function is binary cross entropy (BCE).

V.S	ACC	SENS	SEPC	PREC	RECA	F1-Score	ROC	C.M	EP
0.40	100%	1.0	1.0	100%	100%	100%	1.0	[7 0][0 25]	40
0.30	100%	1.0	1.0	100%	100%	100%	1.0	[8 0][0 24]	40
0.30	94%	1.0	1.0	100%	91.7%	95.652%	0.96	[8 0][2 22]	50

V.S: Validation split, ACC: Accuracy, SENS: Sensitivity, SEPC: specificity, PREC: Precision, RECA: Recall, Roc: ROC (area), C.M: Confusion Matrix, EP: epochs.

Table 5. Comparison between the performance of the existing approaches and the suggested approach.

Author	Method	Accuracy
Ozturk et al. 2020 [35]	Models based on deep learning for binary classification	98.08% and 87.02%
Azemin et al. 2020 [58]	learning-based COVID-19	71.9%
Heidari et al. 2020 [56]	Convolution neural network (CNN)	94.5%
Oh et al. 2020 [57]	statistical method	88.9%
Asnaoui et al. 2021 [65]	inception-ResNetV2	92.18%

In Tables 6 and 7, we compare our suggested model to the relevant cutting-edge techniques. Sethy et al. [37] used 381 chest X-ray images from three groups of identical imaging data (COVID-19, pneumonia, and healthy) in their study on detection. In their studies, they classified data using ResNet50+SVM and attained 95.33% precision. They did not detail specifics about the standards and network requirements.

After making the X-ray picture 200 by 266 pixels big, Apostolopoulos and Mpesiana used the Adam optimizer and the ReLU activation function. Their network includes two hidden layers, one dropout, ten epochs, and a 97.82% success rate. They used deep CNN with ResNet, with the default values of the hyperparameters and the initialization approach [34].

The authors of XCOVNet [113] employed CNN to classify 392 chest X-ray images. (Two sets of the same size as COVID and Normal) and also accomplished a 98.44% accuracy. However, the authors of the cutting-edge publications did not sufficiently specify the details of their experiments, making it difficult to test their model's predictions using our data sets.

Despite producing encouraging findings, our suggested approach has limitations. First, we used two data sets that were readily available; these data sets are described in Section 3. Because COVID-19 symptoms can be very different, the complexity of the model we suggested needs to be checked and confirmed using a larger data set with larger image data sets, and the model needs to be optimized (minimize the number of parameters).

Table 6. Related work comparison only chest X-ray, A.

Author	Method	Image Type	Size Dataset	Accuracy	Covid:Total
Sethy et al. 2020 [37]	Resnet and SVM	Chest X-ray	381 total 127 covid	95.38%	33%
Apostolopoulos et al. 2020 [34]	Deep CNN—ResNet and inception	Chest X-ray	1427 total. 224 covid	97.82%	15.6%
XCOVNet 2021 [113]	CNN	Chest X-ray	392 total. 196 covid	98.44%	50%
Proposed model 2022	CNN with CWB-Cx and Data-Augmentation	Chest X-ray	516 total 102 COVID-19 (data set1)	100%	19.7%
Proposed model 2022	CNN with CWB-CX and Data-Augmentation	Chest X-ray	1583 total 576 COVID-19 (data set2)	100%	37.4%

Table 7. Related work comparison only chest X-ray, B.

Author	Method	Image Type	Size data set	Accuracy	Drawbacks
Hemdan et al. 2020 [13]	COVIDX-Net	Chest Xray	25 COVID-19 (+) 25 COVID-19 (−)	90.0%	Using a dataset that only contains 25 COVID-19 samples.
Wang et al. 2020 [15]	COVID-Net	Chest Xray	358 COVID-19 (+) 8066 COVID-19 (−) 5538 Pneumonia	92.40	Using unbalanced data set 8066 COVID-19 (−). High computational complexity as a result of Pneumonia’s 5538 deep learning trainings.
Ozturk et al. 2020 [35]	DarkCovidNet	Chest Xray	125 COVID-19 (+) 500 No- Findings 125 COVID-19 (+) 500 No-Findings 500 Pneumonia	98.08% and 87.02%	Use of a small number of COVID-19 Samples. High computational complexity as a result of deep learning.
Narin et al. 2021 [64]	Deep CNN ResNet50	Chest Xray	50 COVID-19 (+) 50 COVID-19 (−)	98.0%	Use of a data set including 50 COVID-19 samples, a small number.
Nasiri H. 2022 [114]	DenseNet169+ ANOVA + XGBoost	Chest X-ray	125 COVID-19 (+) 500 No- Findings 125 COVID-19 (+) 500 No-Findings 500 Pneumonia	98.72% and 92.0%	Sensitivity to the ANOVA’s number of features chosen utilizing only a small number of COVID-19 samples
Proposed model (CWB-CX) 2022	CNN with CWB-CX and Data-Augmentation	Chest X-ray	516 total and 102 COVID-19 (data set1) 1583 Normal 576 COVID-19 (data set2)	94% worst 98% average and 100% Best see Table 8	-Needs to be optimized (minimize the number of parameters) -use a medium size data set

4.1. Results and Discussion

The suggest method is applied to two data sets, which are described in Section 3.1 for the two-class classification. The two data set distributions are shown in Figures 1 and 2. The effectiveness is assessed and contrasted using metrics based on the confusion matrix. The proposed model results are compared to the existing state-of-the-art approaches Tables 6 and 7. A confusion matrix is built for 32 examples at each time on the forecasted label of the testing set. We have expressed the model’s success rate in terms of performance metrics like accuracy, F1-score, Accuracy, Sensitivity, and Specificity, which are computed using Equations (6)–(11) [115]. The training is done with different epochs, two loss functions (Binary Cross entropy and categorical cross-entropy), two optimizers (Adam with a learning rate of 0.001, and SGD (learning rate = 0.001, momentum = 0.9), where the results are described in Tables 1–4. In addition, the receiver operating characteristics (ROC) curve is plotted, and the area under the curve (AUC) is calculated. Figure 7 demonstrate how the training accuracy rises as the validation accuracy rises, indicating that the CWB+CX model is not over-fitted. The worst, average and best cases for the proposed model 8 (prediction model, confusion matrix and ROC) are presented in Figures 8–13.

$$Accuracy = \frac{TN + TP}{TN + TP + FN + FP} \quad (6)$$

$$Specificity = \frac{TN}{TN + FP} \tag{7}$$

$$Sensitivity = \frac{TP}{FN + TP} \tag{8}$$

$$Precision = \frac{TP}{FP + TP} \tag{9}$$

$$F1 = \frac{2 * TP}{2 * TP + FP + FN} \tag{10}$$

$$MCC = \frac{(TP * TN) - (FP * FN)}{\sqrt{(TP + FP)(TP + FN)(TN + FP)(TN + FN)}}. \tag{11}$$

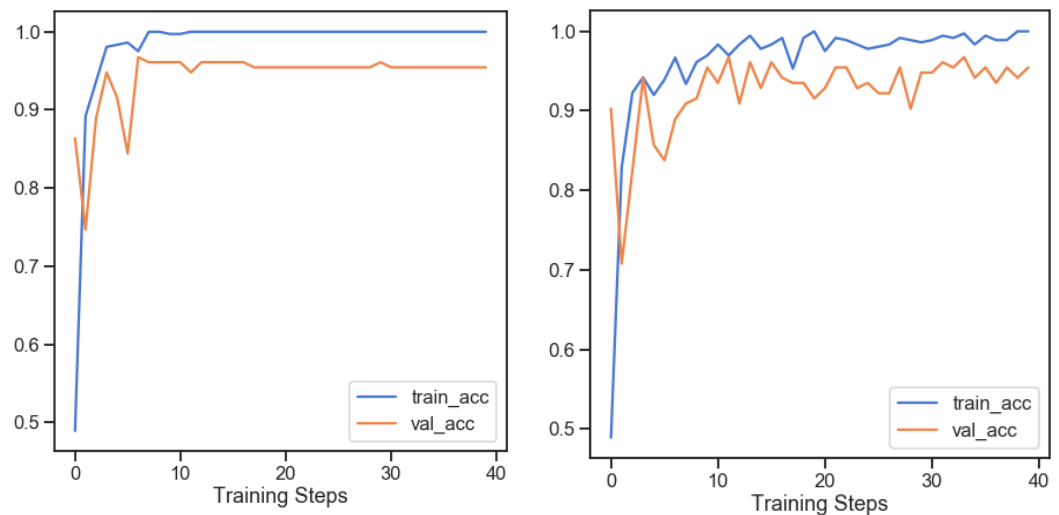


Figure 7. Accuracy (training and validation) 40, 50 epochs.

Figure 7 demonstrate how the training accuracy rises as the validation accuracy rises, indicating that the CWB+CX model is not over-fitted.

In the next Table 8, we summarize the results of our suggested method and the loss function of the worst-case scenario in the Figure 12.

Table 8. AC, SENS, SPEC, PRE, REC and F1-score, for 3 cases worst, average and best cases.

Cases	AC	SENS	SEPC	PRE	REC	F1-Score
Worst	0.94	0.86	0.86	96%	96%	96%
Average	0.97	0.86	0.86	97%	100%	98%
Best	1.00	1.00	1.00	100%	100%	100%

Finally, we summarize the worst, average, and best cases in Table 8, which show that the proposed model attains motivation results to detect COVID-19.

The presentation of the confusion matrix in Figures 9–11 are described below. Figure 9 shows that the actual and predicted COVID-19 values for the examples are 18.75%. Overall, 75% of patients are normal and are predicted to be normal. Normal and anticipated COVID-19 cases are 6.25%. The proportion of COVID-19 and normal-predicting instances is 0%. Figure 10 illustrates the instances of actual and predicted COVID-19 (21.875%). Seventy-five percent of patients are normal and are predicted to be normal. For patients, the normal and expected COVID-19 is 3.125 percent. Furthermore, 0% of instances in COVID-19 are expected to be normal. The examples of real COVID-19 and anticipated COVID-19 are

depicted in Figure 11. Overall, 71.875% of cases are normal and are anticipated to be normal, whereas 0% of patients are normal and have a predicted COVID-19. Figure presents the ROC's worst, average, and best cases.

Covid19 predictions lightweight CNN and class weight balancing model (green: correct, red: incorrect)

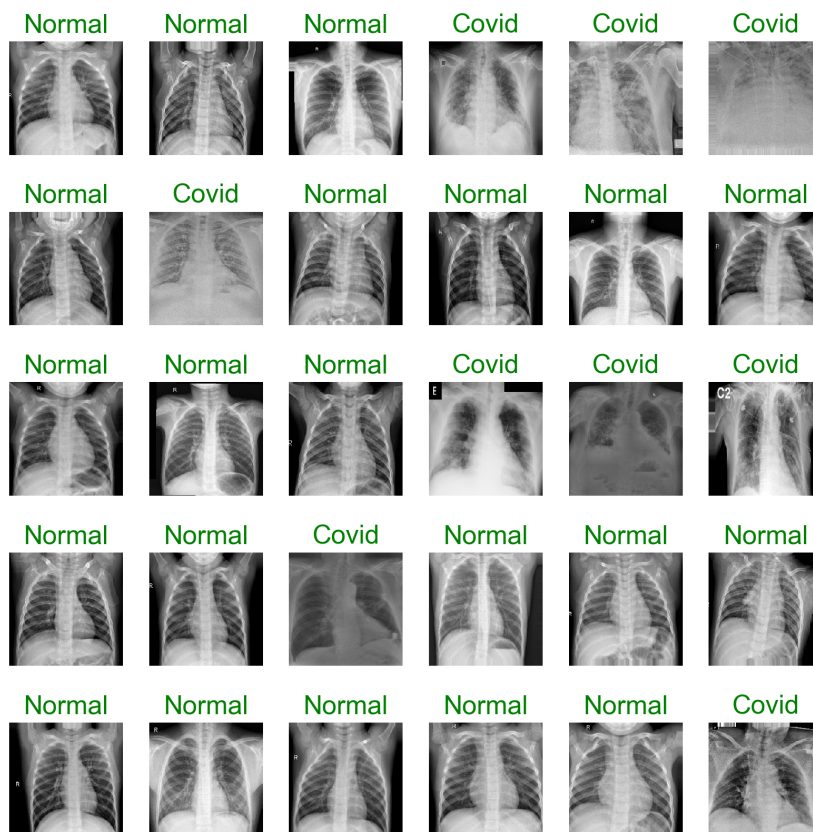


Figure 8. Model prediction best score.

Covid19 predictions lightweight CNN and class weight balancing model (green: correct, red: incorrect)

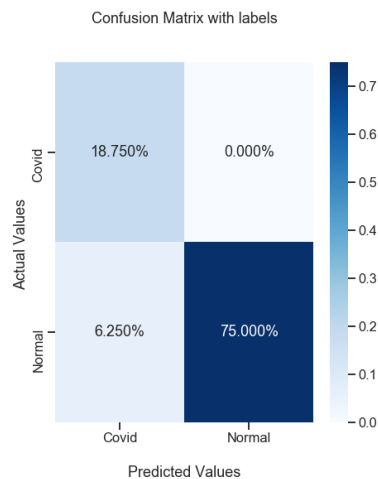
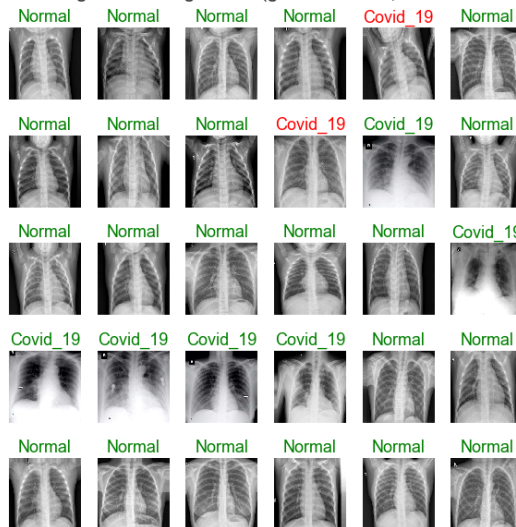


Figure 9. The worst case of the proposed model with Confusion Matrix.

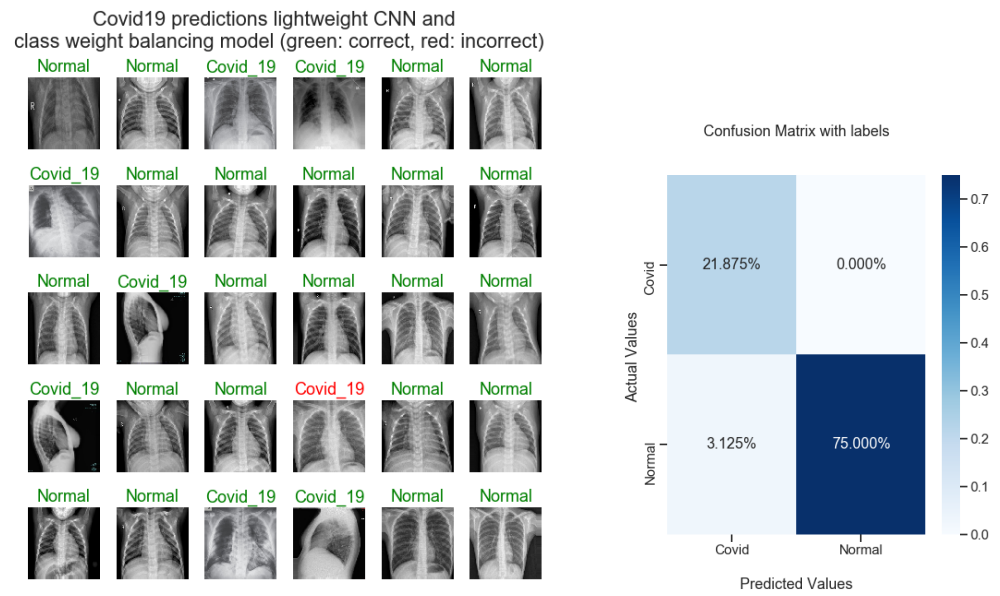


Figure 10. The average case of the proposed model with the Confusion Matrix.

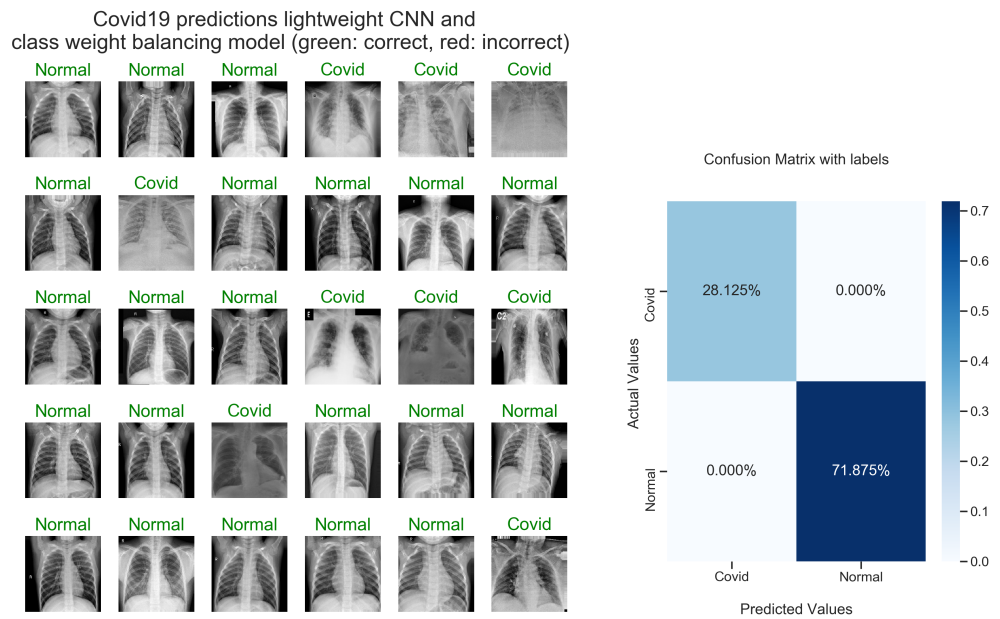


Figure 11. The best case of the proposed model with the Confusion Matrix.

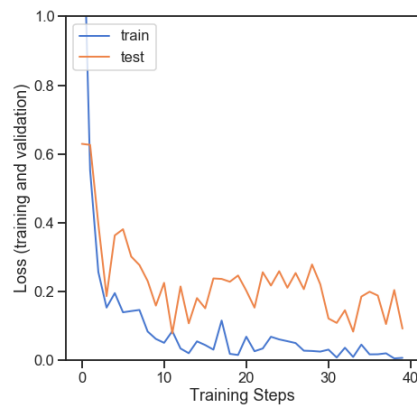


Figure 12. The loss function of the worst case in Table 8.

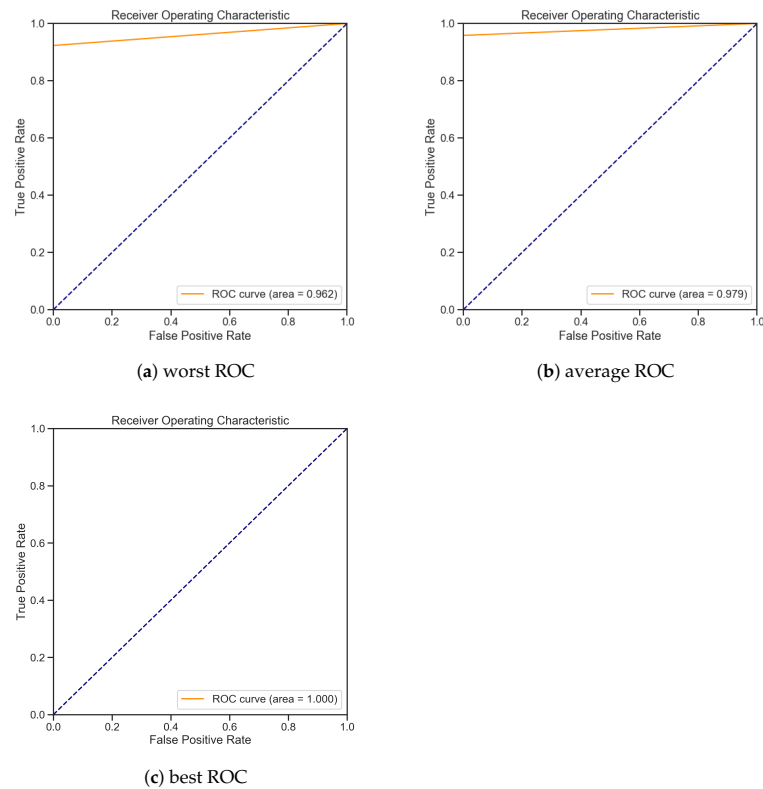


Figure 13. ROC, worst, average and best cases.

4.2. Results Data Set2

Data set 2 consists of 1728 images belonging to two classes for learning and 431 images belonging to two classes for validation. The distribution of the data set is present in Figures 2 and 14. The model in Figure 2 without the dropout layer is used in the experimental data set 1, and the model in Figure 14. The model with the dropout layer is used in experimental data set 2.

In the following section, we present four experimental cases with dropout = 0.3, data augmentation parameters are width shift range = 0.05, zoom range=0.05, shear range = 0.05, height shift range = 0.05, horizontal flip = False, fill mode = 'nearest'), rescale = 1. /255, and validation split = 0.20. The batch-size = 32, where the weight classes for 576 images is 1.874 and for 1583 images is 0.681, the kernel size = 2 × 2, the filters are 64, 64, 128 and 256, and the pooling size is 2 × 2. The total parameters of the model are 32,951,006, and the numbers of the epochs = 50. With Trainable params: 32,951,006.

In the following Table 9, we present the results of four cases. We present case 4 in Table 9, and the optimization loss function, the accuracy function, the confusion matrix, model presentation and Roc curve in the Figures 15–19, respectively.

Table 9. Four cases for data set 2.

Cases	ACC	SENS	SEPC	PREC	RECA	F1-Score	ROC	C.M	M.C.C
case 1	99.3%	1	1	100% 95.65%	97.77%	97.77%	0.978	[9 0][1 22]	0.927
case 2	98.8%	1	1	100%	95.83%	97.87%	0.979	[8 0][1 23]	0.922
case 3	98%	1	1	100%	94.74%	97.29%	0.974	[13 0][1 18]	0.937
case 4	97%	1	1	100%	95.65	97.78%	0.978	[9 0][1 22]	0.927

Case 1: Adam’s learning–rate of 0.001 and a Binary Cross Entropy Loss Function (B.C.E.). Case 2: Adam’s learning–rate of 0.001 and a categorical cross-entropy loss function (C.C.E.). Case 3: S.G.D.’s (learning–rate = 0.001, momentum = 0.9) loss function

is binary cross entropy. Case 4: S.G.D. (learning-rate = 0.001, momentum = 0.9), the loss function is categorical cross-entropy, Matthews correlation coefficient (M.C.C) is defined by Equation (11), ACC, SENS, SEPC, RPEC, RECA, ROC, and C.M are defined in Tables 4 and 9.

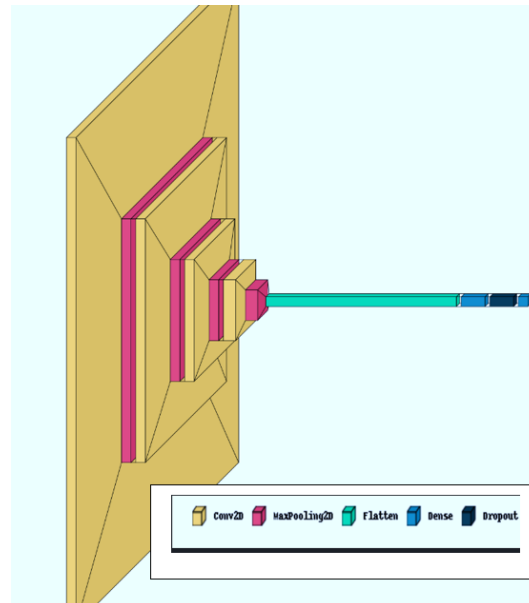


Figure 14. Model with dropout layer.

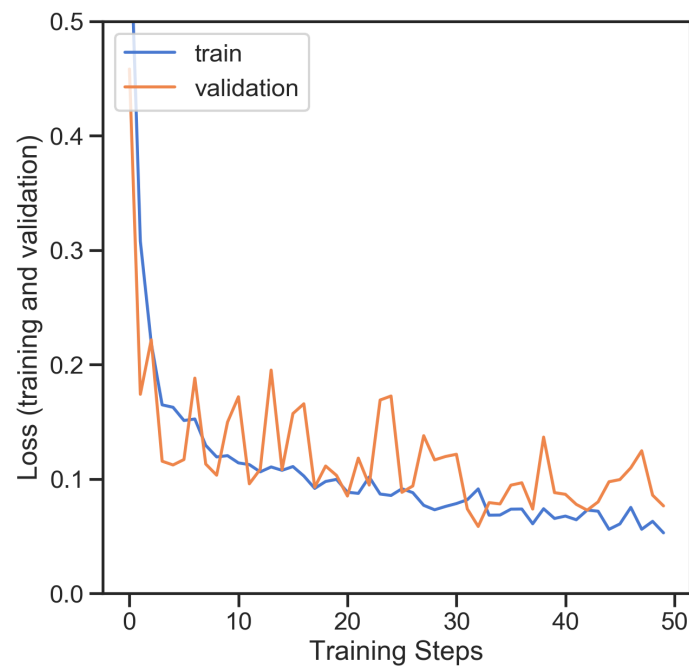


Figure 15. Loss function case 4 in Table 9.

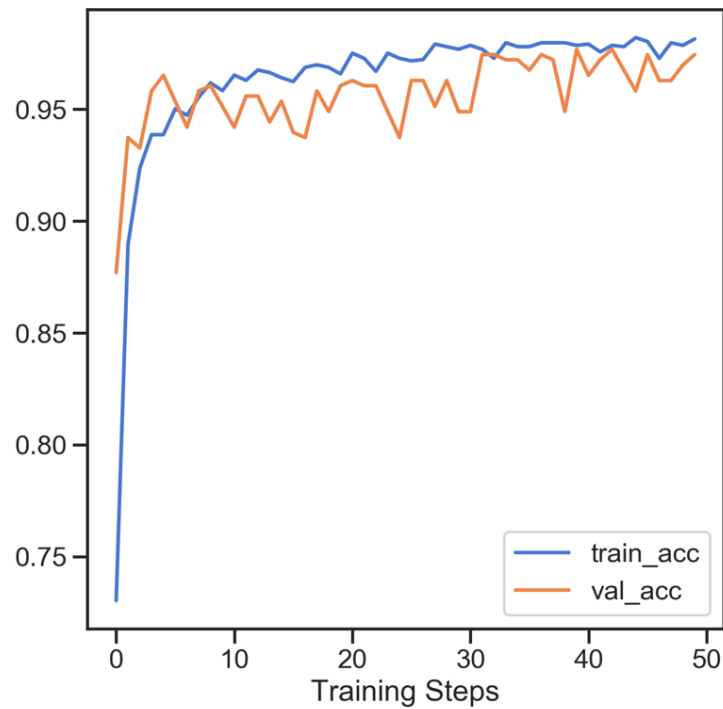


Figure 16. Accuracy function case 4 in Table 9.

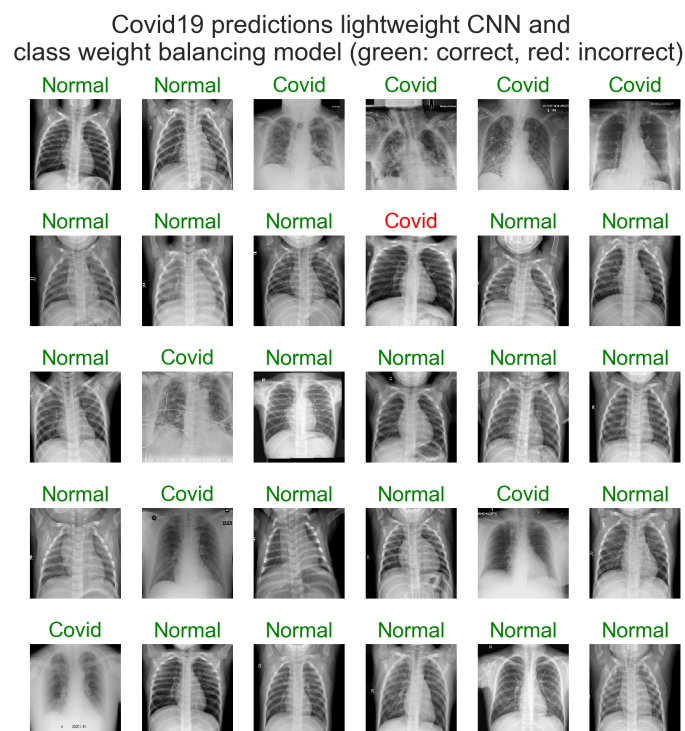


Figure 17. Model prediction case 4 in Table 9.

The Figure 18 confusion matrix shows the TP case’s actual COVID-19 and predicted COVID-19 is (28.125%). TN cases that are normal and predicted normal are 68.750%, FN cases that are normal and predicted COVID-19 are 3.125%, and FP cases that are COVID-19 and predict normal are 0%.

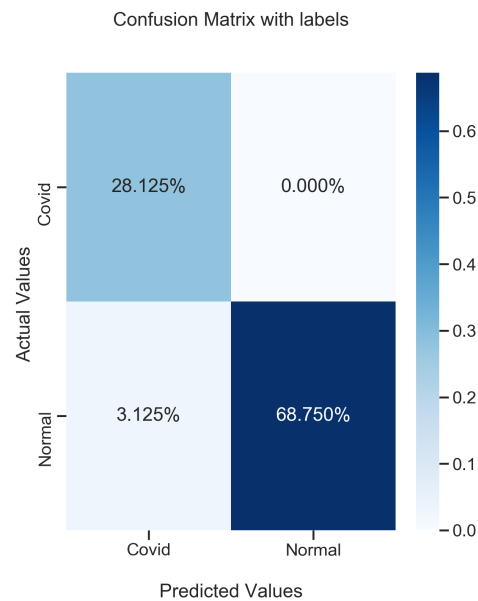


Figure 18. Confusion Matrix case 4 in Table 9.

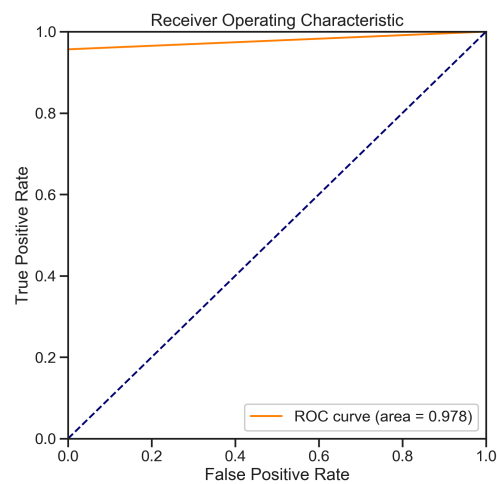


Figure 19. ROC case4 in case 4 in Table 9.

4.3. Model Complexity

In the following, we introduce the proposed model complexity; in machine learning, model complexity is crucial. It is simply the number of independent variables, characteristics, or predictors that a model must consider to make accurate predictions. Our model has 32,951,006 parameters; moreover, the numbers of FLOPS = 1.25 G ($G = 10^9$ floating-point operation). We employed the Keras-flops version 0.1.2 to calculate the number of FLOPs. In Table 10, in millions (M), we provide the number of trainable parameters for the most prevalent deep models. We found that the proposed model needs to be optimized where the number of parameters is 32.95 M, less than both AlexNet and VGG-19, but greater than each of DenesNet, GooleNet, Inception, Xception and MobileNet-V2.

The proposed model (CWB-CX) outperforms several state-of-the-art approaches. In consideration of the problem of class imbalance, the suggested technique has an advantage over previous methods stated in the literature. For the two data sets utilized in the experimental phase, the model (CWB-CX) performs well. Tables 1–4 provide a summary of the findings. The lightweight CWB-CX-based architecture proposed in this paper outperformed [37] and produced a performance comparable to [56,113]. The advantage of the recommended method over existing approaches comes from the fact that it has lower training requirements than transfer learning-based approaches. The classification prob-

lem’s ROC curve illustrates the trade-off between sensitivity and specificity is essential to analyze medical image data. Figure 13 contains the ROC curves for the worst, average, and best-case scenarios. Where the best model is a ROC curve with an AUC value of 1, for the worst, average, and best scenarios, the suggested technique yields AUCs of 0.96, 0.98, and 1.0, respectively. Additionally, data augmentations are employed in conjunction with the parameters shown in Tables 1–4 and 11.

Table 10. The number of trainable parameters for the most prevalent deep models in millions (M).

Model	# Parameters
Alex-Net	62 M
DenseNet	25 M
GooleNet	4 M
Inception V3t	23.6 M
VGG-19	138 M
Xception	22.8 M
MobileNet-V2	3.5 M
Proposed	32.95 M

Figures 9–11 present the worst, average and best cases, respectively. In [32], the author presents the four methods DenseNet-121 (B), B+Model+KNNS, Model Ensemble 1, and Model Ensemble with their Mean AUC and numbers of parameters the best Mean AUC is 93.96, where the mean AUC for the (LW-CNN-CWB) proposed method is 97 and number of parameters is 32.951M. Note that the data sets are different. In [32], the CheXpert dataset [116] is used.

Table 11. Augmentations parameters.

Width	Zoom	Shear	Hight Shift	Fill Mode
0.05	0.05	0.05	0.05	Nearest

Figure 20 summarizes all accuracy for different methods and the proposed model in the three worst, average and best cases. As you can see from Figure 20 and Tables 5–7, our proposed model (CWB-CX) outperforms others in terms of accuracy.

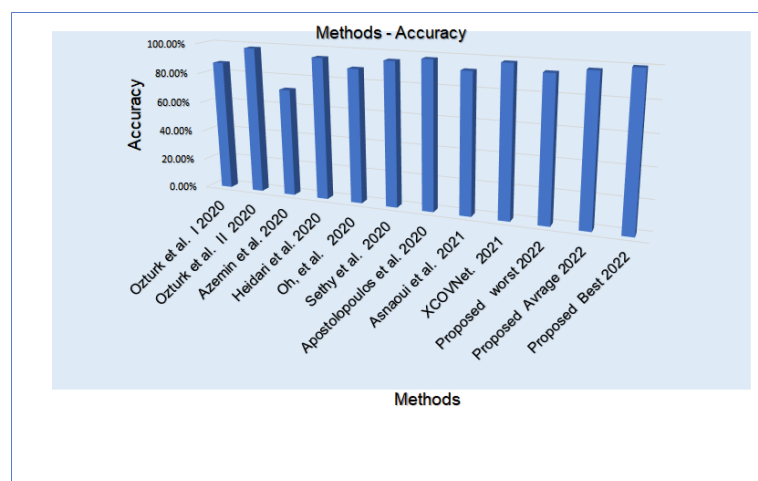


Figure 20. Methods and accuracy. Methods (X-axis) see Table 12.

Table 12. Methods (X-axis) for the Figure 20.

Ozturk et al. I	Ozturk et al. II	Azemin et al.	Heidari et al.	Oh et al.
[35]	[35]	[58]	[56]	[57]
Sethy et al.	Apostolopoulos et al.	Asnaoui et al.	XCOVNet	
[37]	[34]	[65]	[113]	

5. Conclusions and Future Work

In general, in medical imaging data sets, there is an imbalance between the number of normal and disease examples. This study proposes the CWB-CX approach for classifying COVID-19 images and addresses the class imbalance issue. During the period of model training, class weights that penalize the majority class are applied. The trained model is then evaluated using a data set of chest X-ray image data. Parameters based on the confusion matrix are used to assess the results. The efficiency of the suggested model has been analyzed on the criteria like accuracy, specificity, sensitivity, F1-score and MCC. The suggested method accomplished an accuracy of 94% worst, 97% average, and 100% best cases, respectively, and F1 are 96% worst, 98% average and 100% best cases, respectively. The benefit of the suggested mode compared to other state-of-the-art approaches lies in the light of CNN architecture CWB. The suggested model can assist the experts.

The difficulty of our suggested approach necessitates more screening and validation, employing updated data and larger image data sets, and the proposed model needs to be optimized so that the number of parameters is 32.95 million, less than both AlexNet and VGG-19, but greater than each of DenesNet, GooleNet, Inception, Xception, and MobileNet-V2. In the future, we intend to test the proposed model, a lightweight CWB-CX, on chest X-ray images for multi-classification of thoracic disease diagnosis. In future work, we will investigate two databases related to general chest diseases, such as atelectasis, cardiomegaly, consolidation, edema, and pleural effusion, and also apply the proposed model to chest CT images. In addition, we will investigate the implementation of the works of Zhou et al. [32,33] to COVID-19.

Author Contributions: Conceptualization, A.A., S.A.H. and G.A.A.; formal analysis, N.A., S.A.H. and G.A.A. Funding acquisition, N.A. and A.A.; Methodology, N.A. and G.A.A.; Project administration, H.H.; Resources, A.A.; Software, N.A., A.A., S.A.H. and G.A.A.; Supervision, H.H.; Visualization, S.A.H.; Writing—original draft, A.A., S.A.H. and G.A.A.; Writing—review & editing, project administration H.H. All authors listed have made a substantial, direct, and intellectual contribution to the work and approved it for publication. All authors have read and agreed to the published version of the manuscript.

Funding: This research project was funded by Princess Nourah bint Abdulrahman University Researchers Supporting Project number (PNURSP2022R51), Princess Nourah bint Abdulrahman University, Riyadh, Saudi Arabia. The authors thank Natural Sciences and Engineering Research Council of Canada (NSERC), and New Brunswick Innovation Foundation (NBIF) and MITACS for the financial support of the global project. These granting agencies did not contribute in the design of the study and collection, analysis, and interpretation of data.

Data Availability Statement: All data sets found at: <https://www.kaggle.com/prashant268/chest-xray-covid19-pneumonia>, <https://kaggle.com/c/rsna-pneumonia-detection-challenge> (accessed on 10 September 2022).

Acknowledgments: This research project was funded by Princess Nourah bint Abdulrahman University Researchers Supporting Project number (PNURSP2022R51), Princess Nourah bint Abdulrahman University, Riyadh, Saudi Arabia. The authors thank Natural Sciences and Engineering Research Council of Canada (NSERC), and New Brunswick Innovation Foundation (NBIF) and MITACS for the financial support of the global project. These granting agencies did not contribute in the design of the study and collection, analysis, and interpretation of data.

Conflicts of Interest: The authors declare no conflict of interest. The funders had no role in the design of the study; in the collection, analyses, or interpretation of data; in the writing of the manuscript; or in the decision to publish the results.

References

- Phan, L.T.; Nguyen, T.V.; Luong, Q.C.; Nguyen, T.V.; Nguyen, H.T.; Le, H.Q.; Nguyen, T.T.; Cao, T.M.; Pham, Q.D. Importation and human-to-human transmission of a novel coronavirus in Vietnam. *N. Engl. J. Med.* **2020**, *382*, 872–874. [CrossRef] [PubMed]
- Yang, X.; He, X.; Zhao, J.; Zhang, Y.; Zhang, S.; Xie, P. COVID-CT-dataset: A CT scan dataset about COVID-19. *arXiv* **2020**, arXiv:2003.13865.
- Alshazly, H.; Linse, C.; Barth, E.; Martinetz, T. Explainable COVID-19 detection using chest CT scans and deep learning. *Sensors* **2021**, *21*, 455. [CrossRef] [PubMed]
- Abbasi, S.; Naderi, Z.; Amra, B.; Atapour, A.; Dadkhahi, S.A.; Eslami, M.J.; Hajian, M.R.; Hashemi, M.; Hashemi, S.T.; Iraj, B.; et al. Hemoperfusion in patients with severe COVID-19 respiratory failure, lifesaving or not? *J. Res. Med. Sci. Off. J. Isfahan Univ. Med. Sci.* **2021**, *26*, 34.
- Lassau, N.; Ammari, S.; Chouzenoux, E.; Gortais, H.; Herent, P.; Devilder, M.; Soliman, S.; Meyrignac, O.; Talabard, M.P.; Lamarque, J.P.; et al. Integrating deep learning CT-scan model, biological and clinical variables to predict severity of COVID-19 patients. *Nat. Commun.* **2021**, *12*, 1–11. [CrossRef]
- Vahdat, S. The role of IT-based technologies on the management of human resources in the COVID-19 era. *Kybernetes* **2021**. Available online: <https://www.emerald.com/insight/content/doi/10.1108/K-04-2021-0333/full/html> (accessed on 10 September 2022).
- Fang, Y.; Zhang, H.; Xie, J.; Lin, M.; Ying, L.; Pang, P.; Ji, W. Sensitivity of chest CT for COVID-19: Comparison to RT-PCR. *Radiology* **2020**, *296*, E115–E117. [CrossRef]
- Serte, S.; Demirel, H. Deep learning for diagnosis of COVID-19 using 3D CT scans. *Comput. Biol. Med.* **2021**, *132*, 104306. [CrossRef]
- Dinnes, J.; Deeks, J.J.; Berhane, S.; Taylor, M.; Adriano, A.; Davenport, C.; Dittrich, S.; Emperador, D.; Takwoingi, Y.; Cunningham, J.; et al. Rapid, point-of-care antigen and molecular-based tests for diagnosis of SARS-CoV-2 infection. *Cochrane Database Syst. Rev.* **2021**, *8*, CD013705.
- Monica, S.; Singh, P.; Madaan, V. Breast cancer diagnosis using digital image segmentation techniques. *Indian J. Sci. Technol.* **2016**, *9*, 1–5. [CrossRef]
- Gupta, S.; Bharti, V.; Kumar, A. A survey on various machine learning algorithms for disease prediction. *Int. J. Recent Technol. Eng.* **2019**, *7*, 84–87.
- De Moura, J.; García, L.R.; Vidal, P.F.L.; Cruz, M.; López, L.A.; Lopez, E.C.; Novo, J.; Ortega, M. Deep convolutional approaches for the analysis of COVID-19 using chest X-ray images from portable devices. *IEEE Access* **2020**, *8*, 195594–195607. [CrossRef] [PubMed]
- Hemdan, E.E.D.; Shouman, M.A.; Karar, M.E. Covidx-net: A framework of deep learning classifiers to diagnose COVID-19 in X-ray images. *arXiv* **2020**, arXiv:2003.11055.
- Lei, P.; Huang, Z.; Liu, G.; Wang, P.; Song, W.; Mao, J.; Shen, G.; Zhou, S.; Qian, W.; Jiao, J. Clinical and computed tomographic (CT) images characteristics in the patients with COVID-19 infection: What should radiologists need to know? *J. X-ray Sci. Technol.* **2020**, *28*, 369–381. [CrossRef] [PubMed]
- Wang, L.; Lin, Z.Q.; Wong, A. Covid-net: A tailored deep convolutional neural network design for detection of COVID-19 cases from chest X-ray images. *Sci. Rep.* **2020**, *10*, 1–12. [CrossRef] [PubMed]
- Ikedo, M.; Imai, K.; Tabata, S.; Miyoshi, K.; Murahara, N.; Mizuno, T.; Horiuchi, M.; Kato, K.; Imoto, Y.; Iwata, M.; et al. Clinical evaluation of self-collected saliva by RT-qPCR, direct RT-qPCR, RT-LAMP, and a rapid antigen test to diagnose COVID-19. *J. Clin. Microbiol.* **2020**, 1–31. [CrossRef]
- Lisboa Bastos, M.; Tavaziva, G.; Abidi, S.K.; Campbell, J.R.; Haraoui, L.P.; Johnston, J.C.; Lan, Z.; Law, S.; MacLean, E.; Trajman, A.; et al. Diagnostic accuracy of serological tests for COVID-19: Systematic review and meta-analysis. *BMJ* **2020**, *370*, m2516. [CrossRef]
- Silver, D.; Huang, A.; Maddison, C.J.; Guez, A.; Sifre, L.; Van Den Driessche, G.; Schrittwieser, J.; Antonoglou, I.; Panneershelvam, V.; Lanctot, M.; et al. Mastering the game of Go with deep neural networks and tree search. *Nature* **2016**, *529*, 484–489. [CrossRef]
- Brown, T.B.; Mann, B.; Ryder, N.; Subbiah, M.; Kaplan, J.; Dhariwal, P.; Neelakantan, A.; Shyam, P.; Sastry, G.; Askell, A.; et al. Language Models are Few-Shot Learners. *arXiv* **2020**, arXiv:2005.14165.
- OpenAI; Akkaya, I.; Andrychowicz, M.; Chociej, M.; Litwin, M.; McGrew, B.; Petron, A.; Paino, A.; Plappert, M.; Powell, G.; et al. Solving Rubik’s Cube with a Robot Hand. *arXiv* **2019**, arXiv:1910.07113.
- Yu, X.; Kang, C.; Guttery, D.S.; Kadry, S.; Chen, Y.; Zhang, Y.D. ResNet-SCDA-50 for breast abnormality classification. *IEEE/ACM Trans. Comput. Biol. Bioinform.* **2020**, *18*, 94–102. [CrossRef]
- Tamim, N.; Elshrkawey, M.; Abdel Azim, G.; Nassar, H. Retinal blood vessel segmentation using hybrid features and multi-layer perceptron neural networks. *Symmetry* **2020**, *12*, 894. [CrossRef]
- Shaik, N.S.; Cherukuri, T.K. Lesion-aware attention with neural support vector machine for retinopathy diagnosis. *Mach. Vis. Appl.* **2021**, *32*, 1–13. [CrossRef]

24. Bodapati, J.D.; Shaik, N.S.; Naralasetti, V. Composite deep neural network with gated-attention mechanism for diabetic retinopathy severity classification. *J. Ambient. Intell. Humaniz. Comput.* **2021**, *12*, 9825–9839. [[CrossRef](#)]
25. Bodapati, J.D.; Shaik, N.S.; Naralasetti, V. Deep convolution feature aggregation: An application to diabetic retinopathy severity level prediction. *Signal Image Video Process.* **2021**, *15*, 923–930. [[CrossRef](#)]
26. Bodapati, J.D.; Shaik, N.S.; Naralasetti, V.; Mundukur, N.B. Joint training of two-channel deep neural network for brain tumor classification. *Signal Image Video Process.* **2021**, *15*, 753–760. [[CrossRef](#)]
27. Bodapati, J.D.; Shareef, S.N.; Naralasetti, V.; Mundukur, N.B. Msenet: Multi-modal squeeze-and-excitation network for brain tumor severity prediction. *Int. J. Pattern Recognit. Artif. Intell.* **2021**, *35*, 2157005. [[CrossRef](#)]
28. Shaik, N.S.; Cherukuri, T.K. Multi-level attention network: Application to brain tumor classification. *Signal Image Video Process.* **2022**, *16*, 817–824. [[CrossRef](#)]
29. Mohamadou, Y.; Halidou, A.; Kapen, P.T. A review of mathematical modeling, artificial intelligence and datasets used in the study, prediction and management of COVID-19. *Appl. Intell.* **2020**, *50*, 3913–3925. [[CrossRef](#)]
30. Ragab, M.; Alshehri, S.; Aldawsari, H.M.; Noor, A.; Ashary, E.B.; Abou-Taleb, S.A.K.; Abdelazim, G. COVID-19 Identification System Using Transfer Learning Technique With Mobile-NetV2 and Chest X-Ray Images. *Front. Public Health* **2022**, *102*, 1–15. [[CrossRef](#)]
31. Shorten, C.; Khoshgoftaar, T.M.; Furht, B. Deep Learning applications for COVID-19. *J. Big Data* **2021**, *8*, 1–54. [[CrossRef](#)]
32. Zhou, Y.; Zhou, T.; Zhou, T.; Fu, H.; Liu, J.; Shao, L. Contrast-attentive thoracic disease recognition with dual-weighting graph reasoning. *IEEE Trans. Med Imaging* **2021**, *40*, 1196–1206. [[CrossRef](#)] [[PubMed](#)]
33. Zhou, Y.; Huang, L.; Zhou, T.; Shao, L. Many-to-one distribution learning and k-nearest neighbor smoothing for thoracic disease identification. In Proceedings of the AAAI Conference on Artificial Intelligence, Online, 2–9 February 2021; Volume 35, pp. 768–776.
34. Apostolopoulos, I.D.; Mpesiana, T.A. Covid-19: Automatic detection from X-ray images utilizing transfer learning with convolutional neural networks. *Phys. Eng. Sci. Med.* **2020**, *43*, 635–640. [[CrossRef](#)] [[PubMed](#)]
35. Ozturk, T.; Talo, M.; Yildirim, E.A.; Baloglu, U.B.; Yildirim, O.; Acharya, U.R. Automated detection of COVID-19 cases using deep neural networks with X-ray images. *Comput. Biol. Med.* **2020**, *121*, 103792. [[CrossRef](#)] [[PubMed](#)]
36. Waheed, A.; Goyal, M.; Gupta, D.; Khanna, A.; Al-Turjman, F.; Pinheiro, P.R. Covidgan: Data augmentation using auxiliary classifier gan for improved COVID-19 detection. *IEEE Access* **2020**, *8*, 91916–91923. [[CrossRef](#)] [[PubMed](#)]
37. Sethy, P.K.; Behera, S.K. Detection of coronavirus disease (COVID-19) based on deep features and Support Vector Machine. *Preprints* **2020**, *5*, 643–651. [[CrossRef](#)]
38. Qaid, T.S.; Mazaar, H.; Al-Shamri, M.Y.H.; Alqahtani, M.S.; Raweh, A.A.; Alakwaa, W. Hybrid deep-learning and machine-learning models for predicting COVID-19. *Comput. Intell. Neurosci.* **2021**, *2021*, 9996737. [[CrossRef](#)]
39. Abdulkareem, K.H.; Mohammed, M.A.; Salim, A.; Arif, M.; Geman, O.; Gupta, D.; Khanna, A. Realizing an effective COVID-19 diagnosis system based on machine learning and IOT in smart hospital environment. *IEEE Internet Things J.* **2021**, *8*, 15919–15928. [[CrossRef](#)]
40. Khorami, E.; Mahdi Babaei, F.; Azadeh, A. Optimal diagnosis of COVID-19 based on convolutional neural network and red Fox optimization algorithm. *Comput. Intell. Neurosci.* **2021**, *2021*, 4454507. [[CrossRef](#)]
41. Ahmad, F.; Farooq, A.; Ghani, M.U. Deep ensemble model for classification of novel coronavirus in chest X-ray images. *Comput. Intell. Neurosci.* **2021**, *2021*, 8890226. [[CrossRef](#)]
42. Abbas, A.; Abdelsamea, M.M.; Gaber, M.M. Classification of COVID-19 in chest X-ray images using DeTraC deep convolutional neural network. *Appl. Intell.* **2021**, *51*, 854–864. [[CrossRef](#)]
43. Rehman, A.; Iqbal, M.A.; Xing, H.; Ahmed, I. COVID-19 detection empowered with machine learning and deep learning techniques: A systematic review. *Appl. Sci.* **2021**, *11*, 3414. [[CrossRef](#)]
44. Heidari, A.; Navimipour, N.J.; Unal, M.; Toumaj, S. The COVID-19 epidemic analysis and diagnosis using deep learning: A systematic literature review and future directions. *Comput. Biol. Med.* **2021**, *2021*, 105141. [[CrossRef](#)]
45. Park, J.; Kwak, I.Y.; Lim, C. A deep learning model with self-supervised learning and attention mechanism for COVID-19 diagnosis using chest X-ray images. *Electronics* **2021**, *10*, 1996. [[CrossRef](#)]
46. Nasiri, H.; Hasani, S. Automated detection of COVID-19 cases from chest X-ray images using deep neural network and XGBoost. *Radiography* **2022**, *28*, 732–738. [[CrossRef](#)]
47. Heidari, A.; Toumaj, S.; Navimipour, N.J.; Unal, M. A privacy-aware method for COVID-19 detection in chest CT images using lightweight deep conventional neural network and blockchain. *Comput. Biol. Med.* **2022**, *145*, 105461. [[CrossRef](#)]
48. Zheng, Q.; Yang, M.; Yang, J.; Zhang, Q.; Zhang, X. Improvement of generalization ability of deep CNN via implicit regularization in two-stage training process. *IEEE Access* **2018**, *6*, 15844–15869. [[CrossRef](#)]
49. Gao, F.; Yue, Z.; Wang, J.; Sun, J.; Yang, E.; Zhou, H. A novel active semisupervised convolutional neural network algorithm for SAR image recognition. *Comput. Intell. Neurosci.* **2017**, *2017*, 3105053. [[CrossRef](#)]
50. Gu, J.; Wang, Z.; Kuen, J.; Ma, L.; Shahroudy, A.; Shuai, B.; Liu, T.; Wang, X.; Wang, G.; Cai, J.; et al. Recent advances in convolutional neural networks. *Pattern Recognit.* **2018**, *77*, 354–377. doi:10.1016/j.patcog.2017.10.013. [[CrossRef](#)]
51. Pasa, F.; Golkov, V.; Pfeiffer, F.; Cremers, D.; Pfeiffer, D. Efficient deep network architectures for fast chest X-ray tuberculosis screening and visualization. *Sci. Rep.* **2019**, *9*, 1–9. [[CrossRef](#)]
52. Dai, W.c.; Zhang, H.w.; Yu, J.; Xu, H.j.; Chen, H.; Luo, S.p.; Zhang, H.; Liang, L.h.; Wu, X.l.; Lei, Y.; et al. CT imaging and differential diagnosis of COVID-19. *Can. Assoc. Radiol. J.* **2020**, *71*, 195–200. [[CrossRef](#)]

53. Shining a light on COVID-19. *Nature Photonics* **2020**, *14*, 337. [CrossRef]
54. Anderson, M. UV Light Might Keep the World Safe From the Coronavirus—and Whatever Comes Next. *IEEE Spectrum* **2020**. Available online: <https://bio5.org/news/uv-light-might-keep-world-safe-coronavirus-and-whatever-comes-next> (accessed on 10 September 2022).
55. Zhang, Y.; Geng, X.; Tan, Y.; Li, Q.; Xu, C.; Xu, J.; Hao, L.; Zeng, Z.; Luo, X.; Liu, F.; et al. New understanding of the damage of SARS-CoV-2 infection outside the respiratory system. *Biomed. Pharmacother.* **2020**, *127*, 110195. [CrossRef] [PubMed]
56. Heidari, M.; Mirniaharikandehi, S.; Khuzani, A.Z.; Danala, G.; Qiu, Y.; Zheng, B. Improving the performance of CNN to predict the likelihood of COVID-19 using chest X-ray images with preprocessing algorithms. *Int. J. Med. Informatics* **2020**, *144*, 104284. [CrossRef]
57. Oh, Y.; Park, S.; Ye, J.C. Deep learning COVID-19 features on CXR using limited training data sets. *IEEE Trans. Med. Imaging* **2020**, *39*, 2688–2700. [CrossRef] [PubMed]
58. Che Azemin, M.Z.; Hassan, R.; Mohd Tamrin, M.I.; Md Ali, M.A. COVID-19 deep learning prediction model using publicly available radiologist-adjudicated chest X-ray images as training data: Preliminary findings. *Int. J. Biomed. Imaging* **2020**, *2020*, 1–7. [CrossRef]
59. Wang, S.; Kang, B.; Ma, J.; Zeng, X.; Xiao, M.; Guo, J.; Cai, M.; Yang, J.; Li, Y.; Meng, X.; et al. A deep learning algorithm using CT images to screen for Corona Virus Disease (COVID-19). *Eur. Radiol.* **2021**, *31*, 6096–6104. [CrossRef]
60. Laguarda, J.; Hueto, F.; Subirana, B. COVID-19 artificial intelligence diagnosis using only cough recordings. *IEEE Open J. Eng. Med. Biol.* **2020**, *1*, 275–281. [CrossRef]
61. Ai, T.; Yang, Z.; Hou, H.; Zhan, C.; Chen, C.; Lv, W.; Tao, Q.; Sun, Z.; Xia, L. Correlation of chest CT and RT-PCR testing in coronavirus disease 2019 (COVID-19) in China: A report of 1014 cases. *Radiology* **2020**, *296*, E32–E40. [CrossRef]
62. Li, L.; Qin, L.; Xu, Z.; Yin, Y.; Wang, X.; Kong, B.; Bai, J.; Lu, Y.; Fang, Z.; Song, Q.; et al. Using artificial intelligence to detect COVID-19 and community-acquired pneumonia based on pulmonary CT: Evaluation of the diagnostic accuracy. *Radiology* **2020**, *296*, E65–E71. [CrossRef]
63. Li, Y.; Xia, L. Coronavirus disease 2019 (COVID-19): Role of chest CT in diagnosis and management. *AJR Am. J. Roentgenol.* **2020**, *214*, 1280–1286. [CrossRef]
64. Narin, A.; Kaya, C.; Pamuk, Z. Automatic detection of coronavirus disease (COVID-19) using X-ray images and deep convolutional neural networks. *Pattern Anal. Appl.* **2021**, *24*, 1207–1220. [CrossRef] [PubMed]
65. El Asnaoui, K.; Chawki, Y. Using X-ray images and deep learning for automated detection of coronavirus disease. *J. Biomol. Struct. Dyn.* **2021**, *39*, 3615–3626. [CrossRef] [PubMed]
66. Ezzat, D.; Hassani, A.E.; Ella, H.A. An optimized deep learning architecture for the diagnosis of COVID-19 disease based on gravitational search optimization. *Appl. Soft Comput.* **2021**, *98*, 106742. [CrossRef] [PubMed]
67. Kumar, K.S.; Venkatesan, A.; Selvaraj, D.; Raj, A.N.J. Rapid and Accurate Diagnosis of COVID-19 Cases from Chest X-ray Images through an Optimized Features Extraction Approach. *Electronics* **2022**, *11*, 2682. [CrossRef]
68. Vaswani, A.; Shazeer, N.; Parmar, N.; Uszkoreit, J.; Jones, L.; Gomez, A.N.; Kaiser, Ł.; Polosukhin, I. Attention is all you need. *Adv. Neural Inf. Process. Syst.* **2017**, *30*, 1–15.
69. Krizhevsky, A.; Sutskever, I.; Hinton, G.E. Imagenet classification with deep convolutional neural networks. *Commun. ACM* **2017**, *60*, 84–90. [CrossRef]
70. Devlin, J.; Chang, M.W.; Lee, K.; Toutanova, K. Bert: Pre-training of deep bidirectional transformers for language understanding. *arXiv* **2018**, arXiv:1810.04805.
71. Radford, A.; Narasimhan, K.; Salimans, T.; Sutskever, I. Improving language understanding by generative pre-training. *Preprint* **2018**. preprint.
72. Beltagy, I.; Lo, K.; Cohan, A. SciBERT: A pretrained language model for scientific text. *arXiv* **2019**, arxiv:1903.10676.
73. Müller, M.; Salathé, M.; Kummervold, P.E. Covid-twitter-bert: A natural language processing model to analyse covid-19 content on twitter. *arXiv* **2020**, arXiv:2005.07503.
74. Lee, J.; Yoon, W.; Kim, S.; Kim, D.; Kim, S.; So, C.H.; Kang, J. BioBERT: A pre-trained biomedical language representation model for biomedical text mining. *Bioinformatics* **2020**, *36*, 1234–1240. [CrossRef] [PubMed]
75. Lo, K.; Wang, L.L.; Neumann, M.; Kinney, R.; Weld, D.S. S2ORC: The semantic scholar open research corpus. *arXiv* **2019**, arxiv:1911.02782.
76. Wang, L.L.; Lo, K.; Chandrasekhar, Y.; Reas, R.; Yang, J.; Eide, D.; Funk, K.; Kinney, R.; Liu, Z.; Merrill, W.; et al. CORD-19: The covid-19 open research dataset. *arXiv* **2020**, arXiv:2004.10706.
77. Voorhees, E.; Alam, T.; Bedrick, S.; Demner-Fushman, D.; Hersh, W.R.; Lo, K.; Roberts, K.; Soboroff, I.; Wang, L.L. *TREC-COVID: Constructing a Pandemic Information Retrieval Test Collection*; ACM SIGIR Forum; ACM: New York, NY, USA, 2021; Volume 54, pp. 1–12.
78. Thorne, J.; Vlachos, A.; Christodoulopoulos, C.; Mittal, A. Fever: A large-scale dataset for fact extraction and verification. *arXiv* **2018**, arXiv:1803.05355.
79. Dharawat, A.; Lourentzou, I.; Morales, A.; Zhai, C. Drink bleach or do what now? covid-hera: A dataset for risk-informed health decision making in the presence of covid19 misinformation. *arXiv* **2020**, arXiv:2010.08743.
80. Hossain, T.; Logan IV, R.L.; Ugarte, A.; Matsubara, Y.; Singh, S.; Young, S. Detecting COVID-19 misinformation on social media. *Front. Public Health* **2020**. Available online: <https://openreview.net/pdf?id=tRDw11nID9> (accessed on 10 September 2022).

81. Xu, M.; Ouyang, L.; Gao, Y.; Chen, Y.; Yu, T.; Li, Q.; Sun, K.; Bao, F.S.; Safarnejad, L.; Wen, J.; et al. Accurately differentiating COVID-19, other viral infection, and healthy individuals using multimodal features via late fusion learning. *J. Med. Internet Res.* **2020**, *23*, e25535. [CrossRef]
82. Alam, F.; Dalvi, F.; Shaar, S.; Durrani, N.; Mubarak, H.; Nikolov, A.; Da San Martino, G.; Abdelali, A.; Sajjad, H.; Darwish, K.; et al. Fighting the COVID-19 Infodemic in Social Media: A Holistic Perspective and a Call to Arms. In Proceedings of the 15th International Conference on Web and Social Media, Online, 8–10 June 2021; pp. 913–922.
83. Heredia, B.; Prusa, J.; Khoshgoftaar, T. Exploring the effectiveness of twitter at polling the united states 2016 presidential election. In Proceedings of the 2017 IEEE 3rd International Conference on Collaboration and Internet Computing (CIC), San Jose, CA, USA, 15–17 October 2017; pp. 283–290.
84. Heredia, B.; Prusa, J.D.; Khoshgoftaar, T.M. Social media for polling and predicting United States election outcome. *Soc. Netw. Anal. Min.* **2018**, *8*, 1–16. [CrossRef]
85. Brinati, D.; Campagner, A.; Ferrari, D.; Locatelli, M.; Banfi, G.; Cabitza, F. Detection of COVID-19 infection from routine blood exams with machine learning: A feasibility study. *J. Med Syst.* **2020**, *44*, 1–12. [CrossRef]
86. Lopez Rincon, A.; Tonda, A.; Mendoza-Maldonado, L.; Claassen, E.; Garssen, J.; Kraneveld, A.D. Accurate identification of sars-cov-2 from viral genome sequences using deep learning. *Sci. Rep.* **2020**, *11*, 947. [CrossRef]
87. Senior, A.W.; Evans, R.; Jumper, J.; Kirkpatrick, J.; Sifre, L.; Green, T.; Qin, C.; Židek, A.; Nelson, A.W.; Bridgland, A.; et al. Improved protein structure prediction using potentials from deep learning. *Nature* **2020**, *577*, 706–710. [CrossRef] [PubMed]
88. Ahamed, S.; Samad, M. Information mining for COVID-19 research from a large volume of scientific literature. *arXiv* **2020**, arXiv:2004.02085.
89. Zhou, Y.; Wang, F.; Tang, J.; Nussinov, R.; Cheng, F. Artificial intelligence in COVID-19 drug repurposing. *Lancet Digit. Health* **2020**, *2*, e667–e676. [CrossRef] [PubMed]
90. Haque, A.; Milstein, A.; Fei-Fei, L. Illuminating the dark spaces of healthcare with ambient intelligence. *Nature* **2020**, *585*, 193–202. [CrossRef] [PubMed]
91. Russakovsky, O.; Deng, J.; Su, H.; Krause, J.; Satheesh, S.; Ma, S.; Huang, Z.; Karpathy, A.; Khosla, A.; Bernstein, M.; et al. Imagenet large scale visual recognition challenge. *Int. J. Comput. Vis.* **2015**, *115*, 211–252. [CrossRef]
92. Raghu, M.; Zhang, C.; Kleinberg, J.; Bengio, S. Transfusion: Understanding transfer learning for medical imaging. *Adv. Neural Inf. Process. Syst.* **2019**, *32*, 1–22.
93. Topol, E.J. Welcoming new guidelines for AI clinical research. *Nat. Med.* **2020**, *26*, 1318–1320. [CrossRef]
94. Makary, M.A.; Daniel, M. Medical error—The third leading cause of death in the US. *BMJ* **2016**, *353*, i2139. [CrossRef]
95. Wozniak, S. Wozniak: Could a Computer Make a Cup of Coffee? Available online: <https://www.fastcompany.com/1568187/wozniak-could-computer-make-cup-coffee> (accessed on 10 September 2022).
96. Barfoot, T.; Burgner-Kahrs, J.; Diller, E.; Garg, A.; Goldenberg, A.; Kelly, J.; Liu, X.; Naguib, H.E.; Nejat, G.; Schoellig, A.P.; et al. Making sense of the robotized pandemic response: A comparison of global and canadian robot deployments and success factors. *arXiv* **2020**, arXiv:2009.08577.
97. Rieke, N.; Hancox, J.; Li, W.; Milletari, F.; Roth, H.R.; Albarqouni, S.; Bakas, S.; Galtier, M.N.; Landman, B.A.; Maier-Hein, K.; et al. The future of digital health with federated learning. *NPJ Digit. Med.* **2020**, *3*, 1–7. [CrossRef]
98. Zeroual, A.; Harrou, F.; Dairi, A.; Sun, Y. Deep learning methods for forecasting COVID-19 time-Series data: A Comparative study. *Chaos Solitons Fractals* **2020**, *140*, 110121. [CrossRef] [PubMed]
99. Dandekar, R.; Barbasthis, G. Quantifying the effect of quarantine control in Covid-19 infectious spread using machine learning. *MedRxiv* **2020**, preprint.
100. Arik, S.; Li, C.L.; Yoon, J.; Sinha, R.; Epshteyn, A.; Le, L.; Menon, V.; Singh, S.; Zhang, L.; Nikoltchev, M.; et al. Interpretable sequence learning for COVID-19 forecasting. *Adv. Neural Inf. Process. Syst.* **2020**, *33*, 18807–18818.
101. Meiron, E.; Maron, H.; Mannor, S.; Chechik, G. Controlling graph dynamics with reinforcement learning and graph neural networks. In Proceedings of the International Conference on Machine Learning, PMLR, Online, 18–24 July 2021; pp. 7565–7577.
102. Zhao, M.; Jha, A.; Liu, Q.; Millis, B.A.; Mahadevan-Jansen, A.; Lu, L.; Landman, B.A.; Tyska, M.J.; Huo, Y. Faster Mean-shift: GPU-accelerated clustering for cosine embedding-based cell segmentation and tracking. *Med. Image Anal.* **2021**, *71*, 102048. [CrossRef]
103. Zhao, M.; Liu, Q.; Jha, A.; Deng, R.; Yao, T.; Mahadevan-Jansen, A.; Tyska, M.J.; Millis, B.A.; Huo, Y. VoxelEmbed: 3D instance segmentation and tracking with voxel embedding based deep learning. In Proceedings of the International Workshop on Machine Learning in Medical Imaging, Strasbourg, France, 27 September 2021; pp. 437–446.
104. Jin, B.; Cruz, L.; Gonçalves, N. Pseudo RGB-D Face Recognition. *IEEE Sensors J.* **2022**, *22*, 21780–21794. [CrossRef]
105. Akbar, S.; Tariq, H.; Fahad, M.; Ahmed, G.; Syed, H.J. Contemporary Study on Deep Neural Networks to Diagnose COVID-19 Using Digital Posteroanterior X-ray Images. *Electronics* **2022**, *11*, 3113. [CrossRef]
106. Data set2 Description. Available online: <https://www.kaggle.com/prashant268/chest-xray-covid19-pneumonia> (accessed on 10 September 2022).
107. King, G.; Lucas, C.; Nielsen, R.A. The balance-sample size frontier in matching methods for causal inference. *Am. J. Political Sci.* **2017**, *61*, 473–489. [CrossRef]
108. King, G.; Zeng, L. Logistic regression in rare events data. *Political Anal.* **2001**, *9*, 137–163. [CrossRef]
109. Murphy, K.P. *Machine Learning: A Probabilistic Perspective*; MIT Press: Cambridge, MA, USA, 2012.

110. Glorot, X.; Bengio, Y. Understanding the difficulty of training deep feedforward neural networks. In Proceedings of the Thirteenth International Conference on Artificial Intelligence and Statistics, JMLR Workshop and Conference Proceedings, Sardinia, Italy, 13–15 May 2010; pp. 249–256.
111. Chollet, F. A Python Deep Learning Library. Astrophysics Source Code Library. *arXiv* **2015**, arXiv:1212.1916.
112. Abadi, M.; Agarwal, A.; Barham, P.; Brevdo, E.; Chen, Z.; Citro, C.; Corrado, G.S.; Davis, A.; Dean, J.; Devin, M.; et al. Tensorflow: Large-scale machine learning on heterogeneous distributed systems. *arXiv* **2016**, arXiv:1603.04467.
113. Madaan, V.; Roy, A.; Gupta, C.; Agrawal, P.; Sharma, A.; Bologa, C.; Prodan, R. XCOVNet: Chest X-ray image classification for COVID-19 early detection using convolutional neural networks. *New Gener. Comput.* **2021**, *39*, 583–597. [[CrossRef](#)] [[PubMed](#)]
114. Nasiri, H.; Alavi, S.A. A novel framework based on deep learning and ANOVA feature selection method for diagnosis of COVID-19 cases from chest X-ray images. *Comput. Intell. Neurosci.* **2022**, *2022*, 4694567. [[CrossRef](#)] [[PubMed](#)]
115. Hanaa, A.Z.; Gamil, A.A. Segmentation of epithelial human type 2 cell images for the indirect immune fluorescence based on modified quantum entropy. *EURASIP J. Image Video Process.* **2021**, *2021*, 1–19. [[CrossRef](#)]
116. Irvin, J.; Rajpurkar, P.; Ko, M.; Yu, Y.; Ciurea-Ilcus, S.; Chute, C.; Marklund, H.; Haghgoo, B.; Ball, R.; Shpanskaya, K.; et al. Chexpert: A large chest radiograph dataset with uncertainty labels and expert comparison. In Proceedings of the AAAI Conference on Artificial Intelligence, Honolulu, HI, USA, 27 January–1 February 2019; Volume 33, pp. 590–597.